

Mind the Gap: Where Analog Ising Machines Cease to Minimize the Ising Hamiltonian

E.M. Hasantha Ekanayake^{1*}, Arvind R. Venkatakrishnan^{2*}, Francesco Bullo², Nikhil Shukla^{1#}

¹University of Virginia, Charlottesville, VA, USA

²University of California Santa Barbara, Santa Barbara, CA, USA

*Equal Contribution; #Email: ns6pf@virginia.edu

The design of nonlinear dynamical systems whose gradient flows minimize the Ising Hamiltonian has emerged as a compelling paradigm for realizing Ising machines, forming the foundation of architectures including coherent Ising machines, simulated bifurcation machines, oscillator-based Ising machines, and dynamical Ising machines. Here, we identify a fundamental structural feature shared by these systems—a functional gap defined by the separation between the destabilization of the trivial state and the stabilization of Ising-encoded states. We demonstrate that this separation creates a finite parameter interval in which convergence to an Ising-encoded solution is no longer functionally guaranteed, and the resulting evolution is dictated by the spectral structure of the Jacobian at bifurcation. Subsequently, by introducing a hybrid dynamical framework that reshapes the bifurcation topology, we establish a principled pathway for modulating this parameter gap. The parameter gap thus emerges as a unifying structural principle for the analysis, design and optimization of analog Ising machines.

I. INTRODUCTION

The pursuit of efficient solutions to combinatorial optimization problems (COPs) remains a central challenge in computing. Ising machines—computational platforms that minimize the Ising Hamiltonian—have emerged as a promising paradigm. The expressive universality of the Ising model enables diverse combinatorial optimization problems to be encoded into a common energy-minimization framework, with solutions identified as ground-state configurations [1–4].

A diverse range of Ising machines have been realized across physical domains and computational strategies. Of particular interest are those that harness the analog dynamics of physical systems, offering intrinsic parallelism and energy efficiency. Representative examples include Coherent Ising Machines (CIMs) [5–9], Simulated Bifurcation Machines (SBMs) [10], Oscillator-based Ising Machines (OIMs) [11–13], and the recently proposed Dynamical Ising Machines (DIMs) [14]. These platforms are distinguished by the nonlinear mechanisms governing their dynamics, ranging from Kuramoto-type phase coupling in OIMs and conjugate coupling in DIMs to effective $\chi^{(2)}$ and Kerr $\chi^{(3)}$ nonlinearities in CIMs and SBMs. The unifying principle across these architectures is the construction of a dynamical manifold whose ground state encodes the optimal Ising configuration.

Although widely referred to as “Ising machines,” we show in this Letter that these systems do not strictly operate as such across all dynamical regimes. Strikingly, we uncover a previously overlooked regime—where the dynamics deviate from exact minimization of the Ising Hamiltonian—that emerges pervasively across CIMs, SBMs, OIMs, and DIMs alike. We refer to this regime as the *parameter gap*. Most importantly, the system must traverse this parameter gap during operation, which can fundamentally undermine its intended role as a faithful

Ising solver. To address this challenge, we introduce a hybrid framework designed to suppress the effects of non-Ising dynamical regime.

II. MIND THE GAP

To understand the notion of the parameter gap, we first express the nonlinear dynamics of the four architectures within a common gradient-flow framework. Each system evolves according to

$$\dot{x} = -\nabla E(x, \eta, W), \quad (1)$$

where E is an energy function, x denotes the binary state variable, η is a regularization parameter, and W is the weight matrix. Here, we focus on antiferromagnetic spin interactions, for which $W_{ij} = -G_{ij}$, where G is the signed adjacency matrix of the underlying graph, defined such that $G_{ij} = -1$ if an edge exists between nodes i and j , and $G_{ij} = 0$ otherwise, relevant to a broad class of problems including MaxCut, graph coloring, and Maximum Independent Set [3, 15]. By construction, the minimizers of E coincide with the minimizers of the Ising Hamiltonian. Noise is typically included in practice but is omitted here for clarity.

Figure 1 summarizes the characteristics of the four systems and illustrates the dynamics as the regularization parameter η is varied (see Supplementary Note 7 for simulation parameters and experimental settings). A detailed derivation of the dynamics and their mapping to the Ising Hamiltonian is provided in the Supplementary Note 1.

A striking observation emerges: *In the general case, there exists a finite interval of the regularization parameter η , with an intractable upper bound, over which the system dynamics fail to faithfully minimize the Ising Hamiltonian.*

Ising machine	Data	Simulation
DIM	$\eta :$ K_s $E(\phi, \eta, \mathbf{W}) :$ $\frac{K}{2} \sum_{i=1}^N \sum_{j=1}^N W_{ij} \cos(\phi_i + \phi_j) - \frac{K_s}{2} \sum_{i=1}^N \cos(2\phi_i)$ $\Delta_{\text{DIM}}(\mathcal{G}) :$ $\frac{K}{2} \lambda_{\max}(J_{\text{DIM}}^{\{0, \pi\}}(\phi^*)) + \frac{K}{2} \lambda_{\max}(-D - W)$	
OIM	$\eta :$ K_s $E(\phi, \eta, \mathbf{W}) :$ $\frac{K}{2} \sum_{i=1}^N \sum_{j=1}^N W_{ij} \cos(\phi_i - \phi_j) - \frac{K_s}{2} \sum_{i=1}^N \cos(2\phi_i)$ $\Delta_{\text{OIM}}(\mathcal{G}) :$ $\frac{K}{2} \lambda_{\max}(J_{\text{OIM}}^{\{0, \pi\}}(\phi^*)) + \frac{K}{2} \lambda_{\max}(D - W)$	
CIM	$\eta :$ p $E(x, \eta, \mathbf{W}) :$ $\sum_{i=1}^N \left[(-1 + p) \frac{x_i^2}{2} - \frac{x_i^4}{4} \right] + \xi \sum_{j=1}^N W_{ij} x_j$ $\Delta_{\text{CIM}}(\mathcal{G}) :$ $-\lambda_{\max}(\xi W - 3\text{diag}(x_1^{*2}, \dots, x_n^{*2})) + \lambda_{\max}(\xi W)$	
SBM	$\eta :$ p $E(x, \eta, \mathbf{W}) :$ $\sum_{i=1}^N \left[(-\Delta_i + p) \frac{x_i^2}{2} - K_e \frac{x_i^3}{4} \right] + \xi_0 \sum_{j=1}^N W_{ij} x_j$ $\Delta_{\text{SBM}}(\mathcal{G}) :$ $-\lambda_{\max}(\xi_0 W - 3K_e \text{diag}(x_1^{*2}, \dots, x_n^{*2})) + \lambda_{\max}(\xi_0 W)$	

FIG. 1: Comparison of dynamical system formulations for minimizing the Ising Hamiltonian and their key characteristics. Across all models, a finite parameter gap (Δ) emerges in which the system evolution does not correspond to minimization of the Ising ground state in the general case. DIM: Dynamical Ising Machine; OIM: Oscillator Ising Machine; CIM: Coherent Ising Machine; SBM: Simulated Bifurcation Machine. ϕ represents the state variable in DIM and OIM, and x denotes the state variable in SBM and CIM. The parameter K denotes the coupling strength in DIM and OIM, whereas ξ and ξ_0 represent the coupling strength in CIM and SBM, respectively. In SBM, Δ_i represents the positive detuning frequency, and K_e denotes the positive Kerr coefficient.

Starting from $\eta = 0$, none of the considered systems guarantee evolution to a valid Ising state. In fact, in CIMs, SBMs, and DIMs, the dynamics preferentially collapse into a trivial state ($\phi = \frac{\pi}{2}$ in DIM, and $x = 0$ in SBM and CIM) that persists up to a (lower) threshold $\eta_{\min} > 0$ and OIMs to the state $\phi = \frac{\pi}{2}$ for $\eta_{\min} < 0$. Ising solutions are stabilized only once the regularization exceeds a critical threshold η_{\max} , beyond which at least one ground-state configuration becomes stable. Determining η_{\max} , however, requires prior knowledge of all the Ising ground-states (see Supplementary note 2), and is therefore generally intractable.

We refer to this interval of the regularization parameter as the *parameter gap*, defined as

$$\Delta = \eta_{\max} - \eta_{\min}. \quad (2)$$

As detailed in Supplementary Note 2, Δ depends on the

largest eigenvalues of the Jacobian matrices at the fixed points corresponding to an optimal ground state spin configuration (λ_{\max}^{GS}) and the trivial state (λ_{\max}^0). Surprisingly, the parameter gap is pervasive to all the four dynamical systems as observed from Figure 1. In Supplementary Note 2, we provide detailed derivations for the thresholds (η_{\min}, η_{\max}), and establish that the parameter gap must be non-negative i.e., $\eta_{\max} \geq \eta_{\min} \Rightarrow \Delta \geq 0$. Notably, for bipartite graphs the parameter gap vanishes i.e., $\Delta = 0$.

The existence of a parameter gap highlights an intrinsic limitation of such dynamical systems, with direct consequences for its functional capability as Ising machines. During practical operation, the regularization parameter—typically pump power in CIMs and SBMs [9, 10], and second-harmonic injection strength in OIMs and DIMs [11, 14]—is ramped up, forcing the system

to traverse this parameter gap. Within this regime, the trivial state is unstable, and even small perturbations, unavoidable in the presence of noise, can deflect the dynamics toward non-optimal Ising solutions, as explored in the following section. Importantly, the failure to minimize the Ising Hamiltonian within the parameter gap does not stem from breakdown of the gradient-flow dynamics (with $\dot{E} \leq 0$ remaining valid), but rather from the fact that the ground state itself does not correspond to an Ising solution until $\eta \geq \eta_{\max}$.

III. FATE OF THE DYNAMICS IN THE GAP

Since the system must traverse the parameter gap to reach the Ising solutions, we now examine the dynamics within this regime. The destabilization of the trivial state occurs when the largest eigenvalue (of the corresponding Jacobian) crosses zero from negative to positive, rendering the corresponding eigenmode unstable. The system then relaxes in the direction of \mathbf{v}_{\max} , with the associated spin configuration given by $\boldsymbol{\sigma}_{\max} = \text{sign}(\mathbf{v}_{\max})$ [9, 16].

When the parameter gap vanishes ($\Delta = 0$), the destabilization of the trivial state coincides with the stabilization of an optimal Ising configuration. In this case, the largest eigenvalue of the Jacobian evaluated about both the trivial state and the optimal configuration crosses zero at the same value of the control parameter ($\eta_{\Delta=0}$). Crucially, since the optimal Ising configuration now constitutes the system's ground state, the dominant linearized mode—associated with the leading eigenvector of the Jacobian—aligns with this configuration. This alignment can be quantified via the normalized projection $\frac{\boldsymbol{\sigma}^* \cdot \mathbf{v}_{\max}}{\|\boldsymbol{\sigma}^*\| \|\mathbf{v}_{\max}\|} = 1$, where $\boldsymbol{\sigma}^*$ denotes the ground-state Ising configuration.

In fact, we will argue (in Supplementary Note 3) that when $\frac{\boldsymbol{\sigma}_{\max} \cdot \mathbf{v}_{\max}}{\|\boldsymbol{\sigma}_{\max}\| \|\mathbf{v}_{\max}\|} = 1$, the eigenvector corresponding to the largest eigenmode will represent an optimal Ising configuration whose energy is given by, $H = -\frac{N}{2} \lambda_{\max} - \#\mathcal{E}(\mathcal{G})$, where λ_{\max} denotes the largest eigenvalue of the Jacobian corresponding to the trivial state for $\eta_{\Delta=0}$ and $\#\mathcal{E}(\mathcal{G})$ represents the number of edges in the graph \mathcal{G} . Such behavior, where \mathbf{v}_{\max} perfectly aligns with an Ising configuration arises only in special cases, including bipartite graphs (see Supplementary Note 3 for a detailed derivation). From a functional standpoint, this implies that the dynamics converge to the ground state with high probability. We verify this behavior through numerical simulations in Supplementary Note 3, demonstrating that DIMs, OIMs, CIMs, and SBMs consistently converge to the ground state for bipartite graphs.

For generic graphs, however, the parameter gap is nonzero. In this regime, destabilization of the trivial state does not typically coincide with stabilization of an optimal Ising configuration, and the leading eigenvector \mathbf{v}_{\max} of the Jacobian need not align with any ground-state Ising configuration. As the parameter gap increases, additional eigenmodes become unstable before

the Ising ground state is stabilized, introducing multiple directions along which perturbations can grow. Since these subdominant unstable modes typically exhibit even weaker alignment with the optimal Ising configuration [16], their activation further suppresses the probability of converging to the ground state. Together, these observations point to two avenues for improving solution quality: (i) reducing the parameter gap, and (ii) improving the alignment between the dominant Jacobian eigenmode \mathbf{v}_{\max} and an optimal Ising configuration. Interestingly, further on, we show that these two aspects of the dynamics are intricately coupled to each other.

IV. BRIDGING THE GAP

We now explore a pathway to improve the alignment between \mathbf{v}_{\max} and an optimal spin configuration ($\boldsymbol{\sigma}^*$). To understand the foundation of our approach, we consider—using the approach proposed by Wang *et al.*, [9] the degree of synchronization,

$$S(\mathbf{v}_{\max}) = \frac{1}{N} (\mathbf{v}_{\max}^\top \boldsymbol{\sigma}_{\max})^2. \quad (3)$$

where, $\boldsymbol{\sigma}_{\max} = \text{sign}(\mathbf{v}_{\max})$. The significance of this metric, as quantified further on, is that it helps define a lower bound for the dominant eigenvector, \mathbf{v}_{\max} , to point to a state with an energy below a given threshold. Since \mathbf{v}_{\max} is determined by the Jacobian at the trivial solution at the point of bifurcation, improving $S(\mathbf{v}_{\max})$ requires reshaping the eigenbasis of this Jacobian.

To this end, we consider a convex combination of existing dynamics designed to reshape the Jacobian spectrum and selectively enhance the projection of \mathbf{v}_{\max} onto an optimal spin configuration while suppressing competing eigendirections. Specifically, we introduce the Hybrid Ising Machine (HyIM) defined by,

$$\begin{aligned} \dot{\phi}_i = & K \sum_{j=1}^N W_{ij} [\alpha \sin(\phi_i + \phi_j) + (1 - \alpha) \sin(\phi_i - \phi_j)] \\ & - K_s \sin(2\phi_i). \end{aligned} \quad (4)$$

where $\alpha \in [0, 1]$ interpolates between the OIM and DIM limits. As in the pure cases, the HyIM admits an energy function E_{HyIM} whose minimizers correspond to the minimizers of the Ising Hamiltonian (see Supplementary Note 4). Additionally, \mathbf{v}_{\max} can be selectively destabilized while all other eigenmodes remain stable, which is critical to ensuring that the system evolves along the dominant eigenvector at bifurcation. This selective destabilization occurs only for $\alpha \in [\alpha_c, 1]$ (see Supplementary Note 5). Consequently, α_c determines the lower bound on α for which HyIM dynamic will evolve along the dominant eigenmode and relevant to the proposed approach. Computing α_c does not require prior knowledge of the ground state.

The gap in the dynamics can be defined as,

$$\Delta_{\text{HyIM}}(\alpha) = K_{s, \text{HyIM}}^{\{0, \pi\}}(\alpha) - K_{s, \text{HyIM}}^{\{\frac{\pi}{2}\}}(\alpha), \quad (5)$$

and it can be shown that $\Delta_{\text{HyIM}} \geq 0$ (i.e., the gap is non-negative) and convex in $\alpha \in [0, 1]$ (see Supplementary Note 5). The convexity implies that if there exists an $\alpha_0 \in [\alpha_c, 1]$ such that $\Delta_{\text{HyIM}}(\alpha_0) < \Delta_{\text{HyIM}}(\alpha = 1)$, then $\Delta_{\text{HyIM}}(\alpha) \leq \Delta_{\text{HyIM}}(\alpha = 1)$ for all $\alpha \in [\alpha_0, 1]$. While the value of α that gives rise to the minimum parameter gap is not known *a priori*, α provides an additional design knob to optimize the parameter gap; in practice, we observe that the minimum parameter gap does not usually occur at the end point ($\alpha = 1$) implying that tuning the standalone DIM dynamics do not provide the minimum gap. In the following, we will show that reducing the gap impacts the functional aspects of the dynamics as well.

From a functional standpoint, for $\alpha \in [0, \alpha_m^k]$, when

$$S(\mathbf{v}_{\max}) > S_{\text{crit}, k}(\mathbf{v}_{\max}) = 1 - \frac{\Delta H^k}{N \Delta_{\text{HyIM}}(\alpha)}, \quad (6)$$

then, $H(\sigma_{\max}) < H^k$, where H^k denotes the k^{th} excited state, H_0 the ground state, and $\Delta H^k = H^k - H_0$ (see Supplementary Note 6);

Equation (82) provides a quantitative link between synchronization and solution quality: if the dominant eigendirection satisfies the inequality, the resulting spin configuration is guaranteed to lie below the k^{th} excited state. Crucially, the critical threshold $S_{\text{crit}, k}$ decreases as the gap $\Delta_{\text{HyIM}}(\alpha)$ decreases. Therefore, reducing the gap by tuning α reduces the degree of synchronization required for certification of low-energy solutions, thereby increasing the likelihood that \mathbf{v}_{\max} identifies a near-optimal Ising configuration.

Consequently, for k such that $\alpha_m^k > \alpha_c$, if \mathbf{v}_{\max} satisfies Eq. (82), then it must point to a spin configuration σ_{\max} satisfying

$$H(\sigma_{\max}) < H^k. \quad (7)$$

To evaluate the impact of the hybrid dynamics, we test five graphs, G1-G5, from the G-set benchmark [17] each consisting of 800 nodes and 19,176 unweighted edges. Fig. 2(a) shows the evolution of $H(\sigma_{\max}) - H(\sigma^*)$ as function of α . This quantity represents the energy gap between the spin configuration identified by the dominant eigenvector at the bifurcation point and the true ground state. Subsequently, we also solve each graph for varying values of α . Each graph is evaluated over 10 independent trials. Fig. 2(b) shows the box plot distribution of δ which is obtained by first identifying the minimum energy achieved across simulations for each value of α , subtracting this minimum from the corresponding energies, and then summarizing the resulting values as box plots as a function of α .

It can be observed that the Ising energy of the binary state, estimated from the sign of the leading

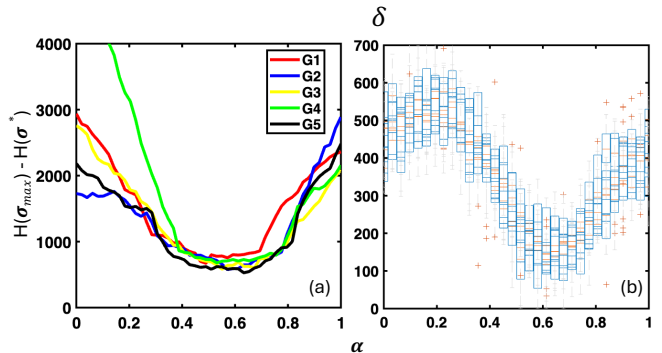


FIG. 2: (a) Evolution of $H(\sigma_{\max}) - H(\sigma^*)$ as a function of α for the first five instances from the Gset benchmark. (b) Box-plot distributions of the δ for different values of α . Each graph is simulated for 10 independent trials.

eigenvector at the bifurcation point—attains a minimum for $\alpha \approx 0.5-0.75$, indicating that the hybrid dynamics can help point the system dynamics evolve towards a lower energy state. More importantly, this improved translates into improved functional performance (i.e., lower Ising energy) as observed in Fig. 2(b).

V. CONCLUSION

We identify a fundamental parameter gap that is intrinsic to a broad class of analog Ising machines. Although these systems evolve as gradient flows, destabilization of the trivial state and stabilization of Ising-encoded solutions occur at distinct thresholds. This separation creates a parameter regime in which optimal spin configurations are not yet stabilized, rendering performance contingent on the structural and design characteristics of the dynamics at bifurcation. We demonstrate that the magnitude of this parameter gap directly constrains computational performance and that reshaping the bifurcation structure through hybrid dynamics can provide a design knob to reduce it. The parameter gap thus emerges as a unifying structural principle for the analysis, design and optimization of analog Ising machines.

ACKNOWLEDGEMENTS

This material is based upon work supported by ARO award W911NF-24-1-0228.

REFERENCES

- [1] F. Barahona, “On the computational complexity of Ising spin glass models,” *Journal of Physics A: Mathematical and General*, vol. 15, no. 10, p. 3241, 1982.
- [2] M. Gu and A. Perales, “Encoding universal computation in the ground states of Ising lattices,” *Physical Review E*, vol. 86, no. 1, p. 011116, 2012.
- [3] A. Lucas, “Ising formulations of many NP problems,” *Frontiers in Physics*, vol. 2, 2014.
- [4] M. K. Bashar, A. Mallick, A. W. Ghosh, and N. Shukla, “Dynamical system-based computational models for solving combinatorial optimization on hypergraphs,” *IEEE Journal on Exploratory Solid-State Computational Devices and Circuits*, vol. 9, no. 1, pp. 21–28, 2023.
- [5] Z. Wang, A. Marandi, K. Wen, R. L. Byer, and Y. Yamamoto, “Coherent Ising machine based on degenerate optical parametric oscillators,” *Physical Review A*, vol. 88, no. 6, p. 063853, 2013.
- [6] A. Marandi, K. Takata, R. Byer, and Y. Yamamoto, “Network of time-multiplexed optical parametric oscillators as a coherent Ising machine,” *Nature Photonics*, vol. 8, p. 937, 2014.
- [7] M. Calvanese Strinati, L. Bello, E. G. Dalla Torre, and A. Pe’er, “Can nonlinear parametric oscillators solve random Ising models?,” *Physical Review Letters*, vol. 126, no. 14, p. 143901, 2021.
- [8] Y. Yamamoto, T. Leleu, S. Ganguli, and H. Mabuchi, “Coherent Ising machines—Quantum optics and neural network perspectives,” *Applied Physics Letters*, vol. 117, no. 16, p. 160501, 2020.
- [9] J. Wang, D. Ebler, K. Y. M. Wong, and J. Sun, “Bifurcation behaviors shape how continuous physical dynamics solves discrete Ising optimization,” *Nature Communications*, vol. 14, no. 1, p. 2510, 2023.
- [10] H. Goto, K. Tatsumura, and A. R. Dixon, “Combinatorial optimization by simulating adiabatic bifurcations in nonlinear Hamiltonian systems,” *Science Advances*, vol. 5, no. 4, p. eaav2372, 2019.
- [11] T. Wang, L. Wu, P. Nobel, and J. Roychowdhury, “Solving combinatorial optimisation problems using oscillator based Ising machines,” *Natural Computing*, vol. 20, no. 2, pp. 287–306, 2021.
- [12] J. Chou, S. Bramhavar, S. Ghosh, and W. Herzog, “Analog coupled oscillator based weighted Ising machine,” *Scientific Reports*, vol. 9, no. 1, p. 14786, 2019.
- [13] J. Vaidya, R. S. Surya Kanthi, and N. Shukla, “Creating electronic oscillator-based Ising machines without external injection locking,” *Scientific Reports*, vol. 12, no. 1, p. 981, 2022.
- [14] E. M. H. E. B. Ekanayake and N. Shukla, “Different paths, same destination: Designing physics-inspired dynamical systems with engineered stability to minimize the Ising Hamiltonian,” *Physical Review Applied*, vol. 24, no. 2, p. 024008, 2025.
- [15] F. Glover, G. Kochenberger, R. Hennig, and Y. Du, “Quantum bridge analytics I: A tutorial on formulating and using QUBO models,” *Annals of Operations Research*, vol. 314, no. 1, pp. 141–183, 2022.
- [16] K. P. Kalinin and N. G. Berloff, “Computational complexity continuum within Ising formulation of NP problems,” *Communications Physics*, vol. 5, p. 20, 2022.
- [17] Y. Ye, “Gset: A collection of graphs for testing algorithms,” *Stanford University*, n.d., accessed: March 2025.
- [18] Y. Cheng, M. K. Bashar, N. Shukla, and Z. Lin, “A control theoretic analysis of oscillator Ising machines,” *Chaos: An Interdisciplinary Journal of Nonlinear Science*, vol. 34, no. 7, 2024.

SUPPLEMENTAL MATERIAL

DEFINITION OF SYMBOLS

The following symbols are used throughout this Supplementary Material:

- G : Signed adjacency matrix of the underlying graph, where $G_{ij} = -1$ if an edge exists between nodes i and j , and $G_{ij} = 0$ otherwise.
- W : Weight matrix, defined by the relation $W_{ij} = -G_{ij}$.
- $\#\mathcal{E}(\mathcal{G})$: The number of edges in the graph \mathcal{G}
- $E(\cdot)$: Energy function.
- \mathbf{J}_f : Jacobian matrix of the dynamical system.
- $S(\cdot)$: Synchronization.
- σ^* : An Ising ground state.
- σ_{\max} : The sign of the dominant eigenvector at the bifurcation point, $\sigma_{\max} = \text{sign}(\mathbf{v}_{\max})$.

SUPPLEMENTARY NOTE 1

Framework for Using Dynamical Systems to Minimize the Ising Hamiltonian

Here, we provide a framework for describing the dynamics of the Ising machines considered in this work. The problem of minimizing the Ising Hamiltonian can be mathematically expressed as,

$$\sigma^*(\mathcal{G}) = \underset{\sigma \in \{-1,1\}^N}{\text{argmin}} -\frac{1}{2}\sigma^\top G\sigma, \quad (8)$$

where \mathcal{G} denotes the underlying graph, G is the adjacency matrix, N is the number of nodes, and $\sigma_i \in \{\pm 1\}^N$ is the Ising spin vector. Computing σ^* is NP-hard in the general case.

The systems (Dynamical Ising Machine (DIM), Oscillator Ising Machine (OIM), Coherent Ising Machine (CIM) and Simulated Bifurcation Machine (SBM)) implement a continuous relaxation of the Ising Hamiltonian by defining an energy function $E(x)$ whose minimizers coincide with those of the Ising Hamiltonian. In many cases, a readout map $h(x)$ is additionally defined such that the optimal Ising configuration is recovered as $\sigma^* = h(x^*)$, where x^* denotes a minimizer of $E(x)$. The associated gradient-flow dynamics, in the presence of noise, can be expressed as,

$$dx(t) = -\nabla_x E(x) dt + dB \quad (9)$$

where dB is Brownian noise. In practice however, the energy function $E(x, \eta; W)$ is parameterized by $\eta \in \mathcal{T} \subseteq \mathbb{R}$ where the mapping to the Ising Hamiltonian is valid only for some range of $\eta \in \mathcal{T}_{\text{compatible}} \subseteq \mathcal{T}$. The compatibility condition is given by

$$\sigma^*(\mathcal{G}) = \{z \in \mathbb{R}^n \mid z = h(x^*), x^* \in \underset{x}{\text{argmin}} E(x, \eta, W)\} \quad (10)$$

for all $\eta \in \mathcal{T}_{\text{compatible}}$, where z denotes the discrete Ising spin vector obtained via the readout map $h(\cdot)$.

SUPPLEMENTARY NOTE 2

Parameter Gap Analysis in Ising Machines: Upper and Lower Bounds

In this section, we compute the lower and upper bounds of the parameter gap for the four models (DIM, OIM, CIM, SBM). The upper bound η_{max} is defined as critical value of η where atleast one ground state becomes stable. The lower bound, η_{min} , defined as critical value of η at which the trivial state loses stability. Since η_{min} may take negative values, whereas only nonnegative values of η are physically relevant in our setting, we define the effective lower bound as, while we only consider a positive η , $\eta_{min} \equiv \max(0, \eta_{min})$

a. Critical Points in the Bifurcation Dynamics of the DIM

The DIM dynamics can be expressed as [14],

$$\frac{d\phi_i}{dt} = K \sum_{j=1, j \neq i}^N W_{ij} \sin(\phi_i + \phi_j) - K_s \sin(2\phi_i). \quad (11)$$

Here, ϕ_i represents the state of the spin i , K denotes the coupling strength and K_s represents the control parameter η in the DIM dynamics. As illustrated in [14], the trivial state of the system, below the critical threshold η_{min} corresponds to the fixed point $\phi^* = (\frac{\pi}{2})\mathbf{1}_N$; and the dynamics converge to the structurally stable [18] fixed point characterized by $\phi^* \in \{0, \pi\}^N$ as the Ising solutions are stabilized when the control parameter K_s exceeds the upper bound η_{max} of the parameter gap.

For the DIM dynamics, the Jacobian of the system dynamics at the equilibrium point ϕ^* is given by,

$$\mathbf{J}_f(\phi^*, K_s) = K \mathbf{J}_{\text{DIM}}(\phi^*) - 2K_s \text{diag}(\cos(2\phi_1^*), \cos(2\phi_2^*), \dots, \cos(2\phi_N^*)) \quad (12)$$

where $\mathbf{J}_{\text{DIM}}(\phi^*)$ can be expressed as,

$$\mathbf{J}_{\text{DIM}}(\phi^*) = \begin{bmatrix} \sum_{j=1, j \neq 1}^N W_{1j} \cos(\phi_1^* + \phi_j^*) & W_{12} \cos(\phi_1^* + \phi_2^*) & \cdots & W_{1N} \cos(\phi_1^* + \phi_N^*) \\ W_{21} \cos(\phi_2^* + \phi_1^*) & \sum_{j=1, j \neq 2}^N W_{2j} \cos(\phi_2^* + \phi_j^*) & \cdots & W_{2N} \cos(\phi_2^* + \phi_N^*) \\ \vdots & \vdots & \ddots & \vdots \\ W_{N1} \cos(\phi_N^* + \phi_1^*) & W_{N2} \cos(\phi_N^* + \phi_2^*) & \cdots & \sum_{j=1, j \neq N}^N W_{Nj} \cos(\phi_N^* + \phi_j^*) \end{bmatrix}. \quad (13)$$

Using the Jacobian defined above, we can define the following:

(a) The critical K_s at which the $\phi^* = (\frac{\pi}{2})\mathbf{1}_N$ becomes unstable:

$$\eta_{min} \equiv K_{s, \text{DIM}}^{\{\frac{\pi}{2}\}} = -\frac{K}{2} \lambda_{\max}(\mathbf{J}_{\text{DIM}}((\frac{\pi}{2})\mathbf{1}_N)) = -\frac{K}{2} \lambda_{\max}(-D - W) \quad (14)$$

where, D , W , and $\lambda_{\max}(\cdot)$ denote the degree matrix, weight matrix, and the dominant eigenvalue of its matrix argument, respectively. Furthermore, for the unweighted anti-ferromagnetically coupled graphs considered in this work, $\mathbf{J}_{\text{DIM}}((\frac{\pi}{2})\mathbf{1}_N)$ can be expressed as,

$$\mathbf{J}_{\text{DIM}}^{\{\frac{\pi}{2}\}} = \mathbf{J}_{\text{DIM}}((\frac{\pi}{2})\mathbf{1}_N) = \begin{bmatrix} -D_1 & -W_{12} & \cdots & -W_{1N} \\ -W_{21} & -D_2 & \cdots & -W_{2N} \\ \vdots & \vdots & \ddots & \vdots \\ -W_{N1} & -W_{N2} & \cdots & -D_N \end{bmatrix},$$

(b) The critical K_s at which atleast one Ising ground state $\phi^* \in \{0, \pi\}^N$ becomes stable is given by,

$$\eta_{max} \equiv K_{s, \text{DIM}}^{\{0, \pi\}} = \min_{\phi \in \text{Ising-ground state}(\mathcal{G})} \frac{K}{2} \lambda_{\max}(J_{\text{DIM}}(\phi^*)) = \frac{K}{2} \lambda_{\max}(J_{\text{DIM}}^{\{0, \pi\}}(\phi^*)). \quad (15)$$

Since the computing $K_{s, \text{DIM}}^{\{0, \pi\}}$ requires knowledge of the ground state, computing this threshold can be computationally intractable. For notational simplicity, we will write $J_{\text{DIM}}^{\{0, \pi\}}(\phi^*) \equiv J_{\text{DIM}}^{\Phi}$. throughout the remainder of this Supplementary Document.

Using the bounds derived above, the parameter gap in the DIM dynamics can expressed as,

$$\begin{aligned} \Delta_{\text{DIM}} &= K_{s, \text{DIM}}^{\{0, \pi\}} - K_{s, \text{DIM}}^{\{\frac{\pi}{2}\}} \\ &= \frac{K}{2} \left[\lambda_{\max}(J_{\text{DIM}}^{\Phi}) - (-\lambda_{\max}(J_{\text{DIM}}^{\{\frac{\pi}{2}\}})) \right] \end{aligned} \quad (16)$$

Establishing $\Delta_{\text{DIM}} \geq 0$

We now establish the ordering $K_{s, \text{DIM}}^{\{\frac{\pi}{2}\}} \leq K_{s, \text{DIM}}^{\{0, \pi\}}$, signifying that the destabilization of the trivial state precedes or coincides with the stabilization of a ground state Ising configuration. Consequently, the parameter gap is non-negative i.e., $\Delta_{\text{DIM}} \geq 0$.

To establish this, we express the Jacobian matrix in terms of the following sets defined as follows: For the fixed point $\phi^* \in \{0, \pi\}^N$, define the set of similar and dissimilar neighbors as,

$$\begin{aligned} \mathcal{N}_i^+(\phi) &= \{j \in \mathcal{N}_i : \cos(\phi_i + \phi_j) = +1\} \\ \mathcal{N}_i^-(\phi) &= \{j \in \mathcal{N}_i : \cos(\phi_i + \phi_j) = -1\}. \end{aligned}$$

Note that $\#\mathcal{N}_i^+(\phi^*) + \#\mathcal{N}_i^-(\phi^*) = D_i$ for all ϕ^* described above. Using this notation, the Jacobian evaluated at a fixed point corresponding to an Ising ground-state configuration $\phi^* \in \{0, \pi\}^N$, as well as at the trivial state $(\frac{\pi}{2})\mathbf{1}_N$, can be written as

$$\begin{aligned} [J_{\text{DIM}}^{\Phi}]_{ij} &= \begin{cases} \#\mathcal{N}_i^+(\phi^*) - \#\mathcal{N}_i^-(\phi^*), & i = j, \\ W_{ij}, & i \neq j, j \in \mathcal{N}_i^+, \\ -W_{ij}, & i \neq j, j \in \mathcal{N}_i^-, \\ 0, & \text{otherwise,} \end{cases} \\ [J_{\text{DIM}}^{\{\frac{\pi}{2}\}}]_{ij} &= \begin{cases} -D_i, & i = j, \\ -W_{ij}, & i \neq j. \end{cases} \end{aligned} \quad (17)$$

Next, to show that $\Delta_{\text{DIM}} \geq 0$, we use the Weyl's inequality. We consider the matrix $\Delta J_{\text{DIM}} = J_{\text{DIM}}^{\Phi} - (-J_{\text{DIM}}^{\{\frac{\pi}{2}\}})$ which can be expressed as,

$$[\Delta J_{\text{DIM}}]_{ij} = \begin{cases} -2\#\mathcal{N}_i^-(\phi^*) & i = j \\ 0 & i \neq j, j \in \mathcal{N}_i^+ \\ -2W_{ij} & i \neq j, j \in \mathcal{N}_i^- \\ 0 & \text{otherwise.} \end{cases} \quad (18)$$

Given a fixed Ising configuration ϕ^* , we define a bipartite graph $\tilde{\mathcal{G}}(\phi^*)$ with weight matrix \tilde{W} specified as

$$\tilde{W}_{ij} = \begin{cases} W_{ij}, & (\phi_i^*, \phi_j^*) \in \{(0, \pi), (\pi, 0)\}, \\ 0, & \text{otherwise.} \end{cases} \quad (19)$$

The graph $\tilde{\mathcal{G}}(\phi^*)$ is thus obtained by restricting the original graph \mathcal{G} to edges connecting nodes whose phases differ by π .

With this construction, the matrix ΔJ_{DIM} can be identified as the negative of the signless Laplacian of the bipartite graph $\tilde{\mathcal{G}}(\phi^*)$. Consequently, ΔJ_{DIM} is negative semidefinite. Moreover, since $\tilde{\mathcal{G}}(\phi^*)$ is bipartite, its signless Laplacian admits a zero eigenvalue, implying that ΔJ_{DIM} has a largest eigenvalue equal to zero (see Supplementary Note 3 for a formal proof).

Applying Weyl's inequality, we obtain

$$\lambda_{\max}(J_{\text{DIM}}^{\Phi}) + \lambda_{\max}\left(J_{\text{DIM}}^{\{\frac{\pi}{2}\}}\right) \geq \lambda_{\max}(\Delta J_{\text{DIM}}) = 0. \quad (20)$$

This establishes that the parameter gap, Δ_{DIM} , is non-negative.

b. Critical Thresholds in Oscillator Ising Machine (OIM)

The dynamics of a Oscillator Ising Machine (OIM) [11] are governed by

$$\frac{d\phi_i}{dt} = K \sum_{j=1, j \neq i}^N W_{ij} \sin(\phi_i - \phi_j) - K_s \sin(2\phi_i), \quad (21)$$

Here, ϕ_i represents the state of the spin i , K denotes the coupling strength and K_s represents the control parameter η in the OIM dynamics. Similar to the DIM, the trivial equilibrium point of the OIM is $(\frac{\pi}{2})\mathbf{1}_N$ and the optimal Ising ground states are a subset of the configurations $\phi^* \in \{0, \pi\}^N$.

To determine the critical thresholds in the OIM, ($K_{s, \text{OIM}}^{\{0, \pi\}}$ and $K_{s, \text{OIM}}^{\{\frac{\pi}{2}\}}$), we evaluate the Jacobian matrices at these fixed points. The Jacobian matrix of the OIM at a configuration ϕ^* is given by,

$$\mathbf{J}_f(\phi^*, K_s) = K J_{\text{OIM}}(\phi^*) - 2K_s \text{diag}(\cos(2\phi_1^*), \cos(2\phi_2^*), \dots, \cos(2\phi_N^*)) \quad (22)$$

where $J_{\text{OIM}}(\phi^*)$ is given by,

$$J_{\text{OIM}}(\phi^*) = \begin{bmatrix} \sum_{j=1, j \neq 1}^N W_{1j} \cos(\phi_1^* - \phi_j^*) & -W_{12} \cos(\phi_1^* - \phi_2^*) & \cdots & -W_{1N} \cos(\phi_1^* - \phi_N^*) \\ -W_{21} \cos(\phi_2^* - \phi_1^*) & \sum_{j=1, j \neq 2}^N W_{2j} \cos(\phi_2^* - \phi_j^*) & \cdots & -W_{2N} \cos(\phi_2^* - \phi_N^*) \\ \vdots & \vdots & \ddots & \vdots \\ -W_{N1} \cos(\phi_N^* - \phi_1^*) & -W_{N2} \cos(\phi_N^* - \phi_2^*) & \cdots & \sum_{j=1, j \neq N}^N W_{Nj} \cos(\phi_N^* - \phi_j^*) \end{bmatrix}. \quad (23)$$

- (a) The critical strength of second harmonic injection, K_s , at which the $\phi^* = (\frac{\pi}{2})\mathbf{1}_N$ becomes unstable can be expressed as,

$$\eta_{min} \equiv K_{s, \text{OIM}}^{\{\frac{\pi}{2}\}} = -\frac{K}{2} \lambda_{\max}(J_{\text{OIM}}((\frac{\pi}{2})\mathbf{1}_N)) = -\frac{K}{2} \lambda_{\max}(D - W) \quad (24)$$

where, D is the degree matrix and W is the adjacency matrix. As the graph Laplacian $L = D - W$ is positive semi-definite, $K_{s, \text{OIM}}^{\{\frac{\pi}{2}\}} \leq 0$.

- (b) The critical K_s at which atleast one Ising ground state $\phi^* \in \{0, \pi\}^N$ becomes stable is given by,

$$\eta_{max} \equiv K_{s, \text{OIM}}^{\{0, \pi\}} = \min_{\phi \in \text{Ising-ground state}(\mathcal{G})} \frac{K}{2} \lambda_{\max}(J_{\text{OIM}}(\phi)) = \frac{K}{2} \lambda_{\max}(J_{\text{OIM}}^{\{0, \pi\}}(\phi^*)). \quad (25)$$

For notational simplicity, we will write $J_{\text{OIM}}((\frac{\pi}{2})\mathbf{1}_N) \equiv J_{\text{OIM}}^{\{\frac{\pi}{2}\}}$ and $J_{\text{OIM}}^{\{0, \pi\}}(\phi^*) \equiv J_{\text{OIM}}^{\Phi}$ throughout the remainder of this Supplementary Document.

Establishing $\Delta_{\text{OIM}} \geq 0$

Similar to the DIM, we establish that $K_{s,\text{OIM}}^{\{\frac{\pi}{2}\}} \leq K_{s,\text{OIM}}^{\{0,\pi\}}$, ensuring that the parameter gap in the OIM is also nonnegative. Following the approach used in the DIM analysis, we express the Jacobian in terms of sets of similar and dissimilar neighbors. For a ground-state configuration $\phi^* \in \{0, \pi\}^N$, we define

$$\mathcal{N}_i^+(\phi) = \{j \in \mathcal{N}_i : \cos(\phi_i - \phi_j) = +1\}, \quad (26)$$

$$\mathcal{N}_i^-(\phi) = \{j \in \mathcal{N}_i : \cos(\phi_i - \phi_j) = -1\}. \quad (27)$$

Note that $\#\mathcal{N}_i^+(\phi^*) + \#\mathcal{N}_i^-(\phi^*) = D_i$.

Using this notation, the Jacobian evaluated at an Ising ground state $\phi^* \in \{0, \pi\}^N$ and at the trivial solution $(\frac{\pi}{2})\mathbf{1}_N$ can be written as

$$[J_{\text{OIM}}^{\Phi}]_{ij} = \begin{cases} \#\mathcal{N}_i^+(\phi^*) - \#\mathcal{N}_i^-(\phi^*), & i = j, \\ -W_{ij}, & i \neq j, j \in \mathcal{N}_i^+, \\ W_{ij}, & i \neq j, j \in \mathcal{N}_i^-, \\ 0, & \text{otherwise,} \end{cases}$$

$$[J_{\text{OIM}}^{\{\frac{\pi}{2}\}}]_{ij} = \begin{cases} D_i, & i = j, \\ -W_{ij}, & i \neq j. \end{cases} \quad (28)$$

We next consider the matrix $\Delta J_{\text{OIM}} = J_{\text{OIM}}^{\Phi} - (-J_{\text{OIM}}^{\{\frac{\pi}{2}\}})$, which can be expressed as

$$[\Delta J_{\text{OIM}}]_{ij} = \begin{cases} 2\#\mathcal{N}_i^+(\phi^*), & i = j, \\ -2W_{ij}, & i \neq j, j \in \mathcal{N}_i^+, \\ 0, & \text{otherwise.} \end{cases} \quad (29)$$

The matrix ΔJ_{OIM} is a graph Laplacian and is therefore positive semidefinite. Applying Weyl's inequality, we obtain

$$\lambda_{\max}(J_{\text{OIM}}^{\Phi}) + \lambda_{\max}(J_{\text{OIM}}^{\{\frac{\pi}{2}\}}) \geq \lambda_{\max}(\Delta J_{\text{OIM}}) \geq 0. \quad (30)$$

This establishes that the OIM parameter gap Δ_{OIM} is nonnegative.

c. Critical Thresholds in Coherent Ising Machine (CIM)

Following the formulation of Wang *et al.* [9], the dynamics of a CIM can be expressed as,

$$\frac{dx_i}{dt} = (-1 + p(t))x_i - x_i^3 + \xi \sum_{j=1}^N W_{ij}x_j, \quad (31)$$

where $x_i \in \mathbb{R}$ denotes the amplitude of the i^{th} oscillator and the parameters p and ξ represent the control parameter ($p \equiv \eta$), and the scaling factor, respectively. At a fixed value of p , the stability of the equilibrium point x^* is determined by the Jacobian matrix,

$$\mathbf{J}_{\mathbf{f}}(x^*, p) = [(-1 + p)I - 3 \text{diag}(x_1^{*2}, \dots, x_n^{*2}) + \xi W] \quad (32)$$

It can be observed that the trivial state $x^* = \mathbf{0}_N$ is always a *unique* fixed point of the CIM dynamics, until it loses stability when p exceeds a critical value given by $\eta_{\min} \equiv p_{\{0\}} = 1 - \lambda_{\max}(\xi W)$. Similarly, the critical value

of p at which at least one optimal Ising configuration, $\{x^*\}^N$, becomes stable can be expressed as, $\eta_{max} \equiv p_{\{\text{Ising}\}} = 1 - \lambda_{\max}(\xi W - 3\text{diag}(x_1^{*2}, \dots, x_n^{*2}))$. Consequently, the parameter gap in the CIM dynamics can be expressed as,

$$\Delta_{\text{CIM}} = p_{\{\text{Ising}\}} - p_{\{0\}} = -\lambda_{\max}(\xi W - 3\text{diag}(x_1^{*2}, \dots, x_n^{*2})) + \lambda_{\max}(\xi W). \quad (33)$$

Furthermore, using Weyl's inequality, we obtain the following relationship,

$$\begin{aligned} -\lambda_{\max}(\xi W - 3\text{diag}(x_1^{*2}, \dots, x_n^{*2})) + \lambda_{\max}(\xi W) &= \lambda_{\min}(-\xi W + 3\text{diag}(x_1^{*2}, \dots, x_n^{*2})) + \lambda_{\max}(\xi W) \\ &\geq \lambda_{\min}(3\text{diag}(x_1^{*2}, \dots, x_n^{*2})) = 3 \min_{1 \leq i \leq n} x_i^{*2} \geq 0. \end{aligned}$$

which shows that the parameter gap is always non-negative.

d. Critical Thresholds in Simulated Bifurcation Machine (SBM)

The dynamics (simplified form) of the SBM can be expressed as [10],

$$\frac{dx_i}{dt} = (-\Delta_i + p(t)) x_i - K_e x_i^3 + \xi_0 \sum_{j=1}^N W_{ij} x_j \quad (34)$$

where Δ_i is the positive detuning frequency between the resonance frequency of the i^{th} oscillator and half the pump frequency, $p(t)$ is the time-dependent two-photon pumping amplitude which serves as the control parameter η , K_e is the positive Kerr coefficient, and ξ_0 is a positive constant with dimension of frequency. For a fixed p , the stability of the equilibrium point x^* is determined by the Jacobian matrix,

$$\mathbf{J}_f(x^*, p) := [(-\Delta_i + p)I - 3K_e \text{diag}(x_1^{*2}, \dots, x_n^{*2}) + \xi_0 W] \quad (35)$$

When the detuning is assumed to be identical across all oscillators, the SBM dynamics reduce to those of the CIM. Under this condition, all results derived for the CIM—including the threshold values and the associated parameter gap—apply directly to the SBM.

SUPPLEMENTARY NOTE 3

Sufficient condition for $\mathbf{v}_{\max} \propto \boldsymbol{\sigma}^*$

In this section, we establish a sufficient condition under which \mathbf{v}_{\max} —the dominant eigenvector at the bifurcation point—aligns with an Ising ground-state configuration $\boldsymbol{\sigma}^*$, i.e., $\mathbf{v}_{\max} \propto \boldsymbol{\sigma}^*$. To establish this sufficient condition, we begin with the Ising Hamiltonian,

$$H(\boldsymbol{\sigma}) = -\frac{1}{2}\boldsymbol{\sigma}^T G \boldsymbol{\sigma} \quad (36)$$

where, $\boldsymbol{\sigma} \in \{-1, 1\}^N$. As detailed in the main text, we consider antiferromagnetic coupling i.e., $W_{ij} = -G_{ij}$, for which $H(\boldsymbol{\sigma}) = -\frac{1}{2}\boldsymbol{\sigma}^T G \boldsymbol{\sigma} = \frac{1}{2}\boldsymbol{\sigma}^T W \boldsymbol{\sigma}$. Using the relationship, $J_{\text{ts}}^* = -D - W \Rightarrow W = -D - J_{\text{ts}}^*$, $H(\boldsymbol{\sigma})$ can be reformulated as,

$$H(\boldsymbol{\sigma}) = -\frac{1}{2}\boldsymbol{\sigma}^T (J_{\text{ts}}^*) \boldsymbol{\sigma} - \frac{1}{2}\boldsymbol{\sigma}^T (D) \boldsymbol{\sigma}. \quad (37)$$

Furthermore, using the identity $\boldsymbol{\sigma}^T D \boldsymbol{\sigma} = \sum_{i=1}^N D_i \sigma_i^2 = 2\#\mathcal{E}(\mathcal{G})$, where $\#\mathcal{E}(\mathcal{G})$ denotes the number of edges of the graph \mathcal{G} , we define,

$$H'(\boldsymbol{\sigma}) = H(\boldsymbol{\sigma}) + \#\mathcal{E}(\mathcal{G}), \quad (38)$$

which corresponds to an offset version of the original Ising Hamiltonian.

Since the matrix J_{ts}^* is symmetric, it admits an orthonormal set of eigenpairs $\{(\lambda_i, \mathbf{v}_i)\}_{i=1}^N$, ordered as $\lambda_{\min} = \lambda_1 \leq \lambda_2 \leq \dots \leq \lambda_N = \lambda_{\max}$. Accordingly, J_{ts}^* admits the spectral decomposition $J_{\text{ts}}^* = \sum_{i=1}^N \lambda_i \mathbf{v}_i \mathbf{v}_i^T$. Substituting this decomposition into the definition of $H'(\boldsymbol{\sigma})$ and simplifying yields,

$$\begin{aligned} H'(\boldsymbol{\sigma}) &= -\frac{1}{2}\boldsymbol{\sigma}^T \left(\sum_{i=1}^N \lambda_i \mathbf{v}_i \mathbf{v}_i^T \right) \boldsymbol{\sigma} \\ &= -\frac{1}{2} \sum_{i=1}^N \lambda_i (\boldsymbol{\sigma}^T \mathbf{v}_i)^2 \\ &= -\frac{1}{2} \left(\lambda_{\max} (\boldsymbol{\sigma}^T \mathbf{v}_{\max})^2 + \sum_{i=1}^{N-1} \lambda_i (\boldsymbol{\sigma}^T \mathbf{v}_i)^2 \right), \end{aligned} \quad (39)$$

To simplify further, note that

$$\sum_{i=1}^N (\boldsymbol{\sigma}^T \mathbf{v}_i)^2 = \|\boldsymbol{\sigma}\|^2 = N, \quad (40)$$

since $\{\mathbf{v}_i\}_{i=1}^N$ forms an orthonormal basis and $\boldsymbol{\sigma} \in \{-1, 1\}^N$. Using this identity, Eq. (39) reduces to

$$\begin{aligned} H'(\boldsymbol{\sigma}) &= -\frac{1}{2} \left(\lambda_{\max} \left(N - \sum_{i=1}^{N-1} (\boldsymbol{\sigma}^T \mathbf{v}_i)^2 \right) + \sum_{i=1}^{N-1} \lambda_i (\boldsymbol{\sigma}^T \mathbf{v}_i)^2 \right) \\ &= -\frac{N}{2} \lambda_{\max} + \frac{1}{2} \sum_{i=1}^{N-1} \Delta_i (\boldsymbol{\sigma}^T \mathbf{v}_i)^2, \end{aligned} \quad (41)$$

where $\Delta_i = \lambda_{\max} - \lambda_i$ and $\Delta_1 \geq \Delta_2 \geq \dots \geq \Delta_{N-1} \geq 0$. Identifying a spin configuration $\boldsymbol{\sigma}$ that minimizes $H'(\boldsymbol{\sigma})$ is equivalent to minimizing the Ising Hamiltonian H , and is therefore NP-hard in general.

Nevertheless, if a spin configuration $\boldsymbol{\sigma}^* \in \{-1, 1\}^N$ satisfies

$$(\boldsymbol{\sigma}^{*\top} \mathbf{v}_i)^2 = 0, \quad i = 1, 2, \dots, N-1, \quad (42)$$

then $H'(\boldsymbol{\sigma}^*) = -\frac{N}{2} \lambda_{\max} \leq H'(\boldsymbol{\sigma})$ for all other $\boldsymbol{\sigma}$, and $\boldsymbol{\sigma}^*$ is an Ising ground state. Consequently, for $\boldsymbol{\sigma}_{\max} = \text{sign}(\mathbf{v}_{\max})$ to be a ground-state configuration, a sufficient condition is

$$(\boldsymbol{\sigma}_{\max}^T \mathbf{v}_i)^2 = 0, \quad i = 1, 2, \dots, N-1. \quad (43)$$

We show that this condition Eq. 43 is satisfied for bipartite graphs.

Bipartite graphs. Let $\mathcal{G} = (\mathcal{V}, \mathcal{E})$ be a connected bipartite graph, and let $G \in \mathbb{R}^{N \times N}$ denote its symmetric adjacency matrix.

Lemma 1 *Let $(\mathbf{v}_i)_{i=1}^N$ be the eigenvectors of the Jacobian matrix J_{ts}^* . We establish the following properties:*

- (a) *The eigenvectors $(\mathbf{v}_i)_{i=1}^N$ of J_{ts}^* form an orthonormal basis of \mathbb{R}^N .*
- (b) *The sign vector $\boldsymbol{\sigma}_{\max}$ coincides (up to normalization) with the dominant eigenvector \mathbf{v}_{\max} of J_{ts}^* .*

An immediate consequence of Lemma 1, it follows that

$$(\boldsymbol{\sigma}_{\max} \cdot \mathbf{v}_i)^2 = \begin{cases} 0, & i = 1, 2, \dots, N-1, \\ N, & i = N, \end{cases}$$

which implies that the sufficient condition stated in Eq. (43) is satisfied. As a result the leading eigenvector at the point of bifurcation can be used to obtain the Ising ground state in bipartite graphs.

Proof.

- (a) Since G is undirected, its weight matrix W is symmetric, i.e., $W = W^\top$. Consequently, $J_{ts}^* = -D - W$ is also symmetric. By the spectral theorem for real symmetric matrices, J_{ts}^* is diagonalizable and admits an orthonormal basis of eigenvectors in \mathbb{R}^n . Eigenvectors associated with distinct eigenvalues are orthogonal, and for repeated eigenvalues, the eigen-space admits an orthonormal bases. Therefore, the eigenvectors of J_{ts}^* can be chosen to form an orthonormal basis of \mathbb{R}^n , establishing property (a).
- (b) For a bipartite graph $G = (V_1 \cup V_2, E)$, the matrix J_{ts}^* admits the block decomposition (refer to the critical points in the bifurcation dynamics of the DIM in the Supplementary Note 2)

$$J_{ts}^* = \begin{pmatrix} -D_1 & -W \\ -W^\top & -D_2 \end{pmatrix} = \begin{pmatrix} -D_1 & -B \\ -B^\top & -D_2 \end{pmatrix},$$

where B denotes the biadjacency matrix and D_1, D_2 are diagonal degree matrices associated with the vertex sets V_1 and V_2 , respectively.

Define the sign vector $\boldsymbol{\sigma} \in \mathbb{R}^N$ by

$$\boldsymbol{\sigma}_i = \begin{cases} +1, & i \in V_1, \\ -1, & i \in V_2. \end{cases}$$

Since G is bipartite, all the neighbors of any vertex $i \in V_1$ lie in V_2 , and vice versa. As a direct consequence of this bipartite structure, the action of J_{ts}^* on \boldsymbol{z} satisfies

$$J_{ts}^* \boldsymbol{\sigma} = - \begin{pmatrix} D_1 & B \\ B^\top & D_2 \end{pmatrix} \begin{pmatrix} \mathbf{1}_m \\ -\mathbf{1}_n \end{pmatrix} = - \begin{pmatrix} D_1 \mathbf{1}_m - B \mathbf{1}_n \\ B^\top \mathbf{1}_m - D_2 \mathbf{1}_n \end{pmatrix} = 0.$$

Hence, $\boldsymbol{\sigma}$ is an eigenvector of J_{ts}^* associated with the eigenvalue 0. Since J_{ts}^* is negative semidefinite—being the negative of the signless Laplacian—this eigenvalue is the largest eigenvalue of the matrix. Therefore, $\boldsymbol{\sigma}$ coincides with the dominant eigenvector \mathbf{v}_{\max} of J_{ts}^* (up to normalization), implying $\boldsymbol{\sigma} = \boldsymbol{\sigma}_{\max}$. This completes the proof of property (b). ■

Simulations: From a functional standpoint, when the dominant eigenvector aligns with an optimal Ising ground-state configuration, the dynamics are expected to converge to the ground state with high probability. To corroborate this, we analyzed a representative randomly-generated bipartite graph with 100 nodes. The graph was solved using each of the four models—OIM, DIM, CIM, and SBM—over 50 independent trials using the same noise amplitude (A_n). In every case, all models consistently found the ground state (Ising-Energy = -764). The corresponding results and the simulation parameters have been summarized in Table I.

TABLE I: Results for a 100-node bipartite graph. Across 50 independent trials, DIM, OIM, CIM, and SBM consistently converged to the optimal Ising-energy ($=-764$).

Model	Ising-Energy	Count	Parameters	Control Parameter ($\eta(t)$)
DIM	-764	50	$K = 1$ $t_{\text{stop}} = 40$ $A_n = 10^{-3}$	$K_s(t) = \frac{4t}{t_{\text{stop}}}$
OIM	-764	50	$K = 1$ $t_{\text{stop}} = 40$ $A_n = 10^{-3}$	$K_s(t) = \frac{4t}{t_{\text{stop}}}$
CIM	-764	50	$\xi = 0.05$ $t_{\text{stop}} = 40$ $A_n = 10^{-3}$	$p(t) = \frac{4t}{t_{\text{stop}}}$
SBM	-764	50	$K_e = 1.0$ $\xi_0 = 0.05$ $\Delta = 1$ $t_{\text{stop}} = 40$ $A_n = 10^{-3}$	$p(t) = \frac{4t}{t_{\text{stop}}}$

SUPPLEMENTARY NOTE 4

Dynamics of the Hybrid Ising Machine (HyIM)

Here, we establish that the HyIM dynamics minimize an energy function whose minimizers coincide with those of the Ising Hamiltonian. Consider the phase dynamics

$$\frac{d\phi_i}{dt} = K \sum_{\substack{j=1 \\ j \neq i}}^N W_{ij} \left[\alpha \sin(\phi_i + \phi_j) + (1 - \alpha) \sin(\phi_i - \phi_j) \right] - K_s \sin(2\phi_i), \quad (44)$$

with $\alpha \in [0, 1]$. Define the energy function

$$E(\phi) = \frac{K}{2} \sum_{\substack{i,j=1 \\ j \neq i}}^N W_{ij} \left[\alpha \cos(\phi_i + \phi_j) + (1 - \alpha) \cos(\phi_i - \phi_j) \right] - \frac{K_s}{2} \sum_{i=1}^N \cos(2\phi_i). \quad (45)$$

Computing the gradient of $E(\phi)$ yields

$$\begin{aligned} \frac{\partial E}{\partial \phi_k} &= -\frac{K}{2} \sum_{\substack{l=1 \\ l \neq k}}^N W_{kl} \left[\alpha \sin(\phi_k + \phi_l) + (1 - \alpha) \sin(\phi_k - \phi_l) \right] \\ &\quad - \frac{K}{2} \sum_{\substack{l=1 \\ l \neq k}}^N W_{lk} \left[\alpha \sin(\phi_l + \phi_k) - (1 - \alpha) \sin(\phi_l - \phi_k) \right] + K_s \sin(2\phi_k). \end{aligned} \quad (46)$$

Since $W_{kl} = W_{lk}$ and $\sin(\phi_l \pm \phi_k) = \pm \sin(\phi_k \pm \phi_l)$, the two sums are identical, giving

$$\frac{\partial E}{\partial \phi_k} = -K \sum_{\substack{l=1 \\ l \neq k}}^N W_{kl} \left[\alpha \sin(\phi_k + \phi_l) + (1 - \alpha) \sin(\phi_k - \phi_l) \right] + K_s \sin(2\phi_k). \quad (47)$$

Comparing with Eq. (44), we obtain the gradient-flow relation

$$\frac{d\phi_k}{dt} = -\frac{\partial E}{\partial \phi_k}. \quad (48)$$

Consequently,

$$\frac{dE}{dt} = \sum_{k=1}^N \frac{\partial E}{\partial \phi_k} \frac{d\phi_k}{dt} = -\sum_{k=1}^N \left(\frac{d\phi_k}{dt} \right)^2 \leq 0, \quad (49)$$

and the system performs gradient descent on $E(\phi)$.

When each phase settles at 0 or π (so that $\cos(2\phi_i) = 1$), the energy reduces to

$$E(\phi) = \frac{K}{2} \sum_{\substack{i,j=1 \\ j \neq i}}^N W_{ij} \left[\alpha \cos(\phi_i + \phi_j) + (1 - \alpha) \cos(\phi_i - \phi_j) \right] - \frac{K_s}{2} N, \quad (50)$$

where $-\frac{K_s}{2} N$ is a constant offset. By choosing $K = 1$, Eq. (45) becomes equivalent to the Ising Hamiltonian up to an additive constant, and therefore shares the same minimizers.

SUPPLEMENTARY NOTE 5

Properties of parameter gap in the HyIM dynamics

The HyIM dynamics can be expressed as,

$$\frac{d\phi_i}{dt} = K \sum_{j=1}^N W_{ij} [\alpha \sin(\phi_i + \phi_j) + (1 - \alpha) \sin(\phi_i - \phi_j)] - K_s \sin(2\phi_i). \quad (51)$$

The Jacobian matrix of this system is given by

$$\mathbf{J}_f(\phi^*, K_s) = K J_{\text{HyIM}}(\phi^*, \alpha) - 2K_s \text{diag}(\cos(2\phi_1^*), \dots, \cos(2\phi_N^*)) \quad (52)$$

where the matrix $J_{\text{HyIM}}(\phi^*, \alpha)$ is defined as,

$$[J_{\text{HyIM}}(\phi^*, \alpha)]_{ij} = \begin{cases} \alpha K \sum_{k=1}^N W_{ik} \cos(\phi_i^* + \phi_k^*) + (1 - \alpha) K \sum_{k=1}^N W_{ik} \cos(\phi_i^* - \phi_k^*) & i = j \\ \alpha K W_{ij} \cos(\phi_i^* + \phi_j^*) - (1 - \alpha) K W_{ij} \cos(\phi_i^* - \phi_j^*) & i \neq j. \end{cases} \quad (53)$$

It can be observed that

$$J_{\text{HyIM}}(\phi^*, \alpha) = \alpha J_{\text{DIM}}(\phi^*, \alpha) + (1 - \alpha) J_{\text{OIM}}(\phi^*, \alpha), \quad (54)$$

implying that the Jacobian is a linear combination of the Jacobians of the OIM and the DIM dynamics. Consequently, the parameter gap can then be defined using the same approach as that used for calculating parameter gap in the OIM and DIM dynamics. Specifically, the critical K_s at which the ground state σ^* becomes stable can be expressed as,

$$K_{s, \text{HyIM}}^{\{0, \pi\}}(\alpha) = \min_{\phi \in \text{Ising-ground state}(G)} \frac{K}{2} \lambda_{\max}(J_{\text{HyIM}}(\phi^*, \alpha)) = \frac{K}{2} \lambda_{\max}(J_{\text{HyIM}}^{\{0, \pi\}}(\phi^*, \alpha)), \quad (55)$$

while the threshold at which the trivial $(\frac{\pi}{2})\mathbf{1}_N$ state loses stability is given by,

$$K_{s, \text{HyIM}}^{\{\frac{\pi}{2}\}}(\alpha) = -\frac{K}{2} \lambda_{\max}(J_{\text{HyIM}}((\frac{\pi}{2})\mathbf{1}_N, \alpha)) = -\frac{K}{2} \lambda_{\max}((1 - 2\alpha)D - W). \quad (56)$$

The parameter gap, therefore, can be calculated as,

$$\begin{aligned} \Delta_{\text{HyIM}}(\alpha) &= K_{s, \text{HyIM}}^{\{0, \pi\}}(\alpha) - K_{s, \text{HyIM}}^{\{\frac{\pi}{2}\}}(\alpha) \\ &= \frac{K}{2} \left[\lambda_{\max}(J_{\text{HyIM}}^{\{0, \pi\}}(\phi^*, \alpha)) - (-\lambda_{\max}((1 - 2\alpha)D - W)) \right]. \end{aligned} \quad (57)$$

Next we analyze key properties of the parameter gap defined above in Eq. (57).

Lemma 2 *The parameter gap $\Delta_{\text{HyIM}}(\alpha)$ is non-negative and convex in $\alpha \in [0, 1]$.*

Proof. We first demonstrate that the parameter gap is non-negative. We proceed in a similar manner to the analysis of this property in OIMs and DIMs. Define the matrix,

$$\begin{aligned}
\Delta J_{\text{HyIM}}(\phi^*, \alpha) &= J_{\text{HyIM}}^{\{0, \pi\}}(\phi^*, \alpha) + J_{\text{HyIM}}\left(\left(\frac{\pi}{2}\right)\mathbf{1}_N, \alpha\right) \\
&= J_{\text{HyIM}}^{\{0, \pi\}}(\phi^*, \alpha) + \left[(1 - 2\alpha)D - W\right] \\
&= \begin{cases} \alpha(\#\mathcal{N}_i^+(\phi^*) - \#\mathcal{N}_i^-(\phi^*)) + (1 - \alpha)(\#\mathcal{N}_i^+(\phi^*) - \#\mathcal{N}_i^-(\phi^*)) + (1 - 2\alpha)D & i = j \\ \alpha W_{ij} + (1 - \alpha)(-W_{ij}) - W_{ij} & i \neq j, j \in \mathcal{N}_i^+ \\ \alpha(-W_{ij}) + (1 - \alpha)W_{ij} - W_{ij} & i \neq j, j \in \mathcal{N}_i^- \\ 0 & \text{otherwise} \end{cases} \\
&= \begin{cases} (\#\mathcal{N}_i^+(\phi^*) - \#\mathcal{N}_i^-(\phi^*)) + (1 - 2\alpha)(\#\mathcal{N}_i^+(\phi^*) + \#\mathcal{N}_i^-(\phi^*)) & i = j \\ 2\alpha W_{ij} - 2W_{ij} & i \neq j, j \in \mathcal{N}_i^+ \\ -2\alpha W_{ij} & i \neq j, j \in \mathcal{N}_i^- \\ 0 & \text{otherwise} \end{cases} \\
&= \begin{cases} 2\#\mathcal{N}_i^+(\phi^*) - 2\alpha(\#\mathcal{N}_i^+(\phi^*) + \#\mathcal{N}_i^-(\phi^*)) & i = j \\ 2\alpha W_{ij} - 2W_{ij} & i \neq j, j \in \mathcal{N}_i^+ \\ -2\alpha W_{ij} & i \neq j, j \in \mathcal{N}_i^- \\ 0 & \text{otherwise} \end{cases}
\end{aligned}$$

By selecting a vector \mathbf{x} whose components satisfy $\mathbf{x}_i = \mathbf{x}_j$ for all $j \in \mathcal{N}_i^+(\phi^*)$ and $\mathbf{x}_i = -\mathbf{x}_j$ for all $j \in \mathcal{N}_i^-(\phi^*)$, it follows directly that $\Delta J_{\text{HyIM}}(\phi^*, \alpha) \mathbf{x} = \mathbf{0}$, which implies that $\Delta J_{\text{HyIM}}(\phi^*, \alpha)$ has a zero eigenvalue. Using Weyl's inequality and Eq. (58), we obtain

$$\lambda_{\max}(J_{\text{HyIM}}^{\{0, \pi\}}(\phi^*, \alpha)) + \lambda_{\max}((1 - 2\alpha)D - W) \geq \lambda_{\max}(J_{\text{HyIM}}^{\{0, \pi\}}(\phi^*, \alpha) + ((1 - 2\alpha)D - W)) \geq 0.$$

This establishes that the parameter gap $\Delta_{\text{HyIM}}(\alpha)$ is non-negative.

Next, we show that $\Delta_{\text{HyIM}}(\alpha)$ is convex in $\alpha \in [0, 1]$. To establish this, we prove that,

$$G(\beta x + (1 - \beta)y) \leq \beta G(x) + (1 - \beta)G(y), \forall x, y, \beta \in [0, 1] \quad (58)$$

Using Eq. (54),

$$J_{\text{HyIM}}(\phi^*, \beta x + (1 - \beta)y) = \beta J_{\text{HyIM}}(\phi^*, x) + (1 - \beta)J_{\text{HyIM}}(\phi^*, y).$$

Since the largest eigenvalue $\lambda_{\max}(M)$ is a convex function of the matrix M , for any $\beta \in [0, 1]$ we have

$$\lambda_{\max}(J_{\text{HyIM}}(\phi^*, \beta x + (1 - \beta)y)) \leq \beta \lambda_{\max}(J_{\text{HyIM}}(\phi^*, x)) + (1 - \beta) \lambda_{\max}(J_{\text{HyIM}}(\phi^*, y)). \quad (59)$$

It follows that $G(\alpha)$ is convex for $\alpha \in [0, 1]$, which concludes the proof. \blacksquare

Threshold α_c to achieve $K_s^{\{\frac{\pi}{2}\}} \geq 0$

We establish the critical value of α that ensures stability of the trivial state in the absence of regularization, i.e., for $K_s = 0$. Ensuring $K_s \geq 0$ is significant because, under this condition, the dynamics evolve along the dominant eigenmode at the point where the trivial state loses stability.

We first show that the critical threshold $K_{s, \text{OIM-DIM}}^{\{\frac{\pi}{2}\}}(\alpha)$ is nondecreasing in α . Recall that, for the HyIM dynamics, the Jacobian evaluated at the trivial state yields

$$K_{s, \text{HyIM}}^{\{\frac{\pi}{2}\}}(\alpha) = -\frac{K}{2} \lambda_{\max}((1 - 2\alpha)D - W). \quad (60)$$

Thus, monotonicity of $K_{s, \text{HyIM}}^{\{\frac{\pi}{2}\}}(\alpha)$ follows from the monotonicity of $\lambda_{\max}((1 - 2\alpha)D - W)$.

Consider any $0 \leq \alpha_1 \leq \alpha_2 \leq 1$. Then,

$$\begin{aligned} \lambda_{\max}((1 - 2\alpha_1)D - W) - \lambda_{\max}((1 - 2\alpha_2)D - W) &= \lambda_{\max}((1 - 2\alpha_1)D - W) + \lambda_{\min}(-(1 - 2\alpha_2)D + W) \\ &\geq \lambda_{\min}(2(\alpha_2 - \alpha_1)D) \\ &= 2(\alpha_2 - \alpha_1) \min_{1 \leq i \leq N} d_i \geq 0, \end{aligned} \quad (61)$$

where, the inequality follows from Weyl's eigenvalue inequality. Equation (61) shows that $\lambda_{\max}((1 - 2\alpha)D - W)$ is nonincreasing in α , and hence $K_{s, \text{HyIM}}^{\{\frac{\pi}{2}\}}(\alpha)$ is nondecreasing in α .

To define the critical value $\alpha_c \in [0, 1]$, note that

$$K_{s, \text{HyIM}}^{\{\frac{\pi}{2}\}}(0) = K_{s, \text{OIM}}^{\{\frac{\pi}{2}\}} < 0, \quad K_{s, \text{HyIM}}^{\{\frac{\pi}{2}\}}(1) = K_{s, \text{DIM}}^{\{\frac{\pi}{2}\}} > 0. \quad (62)$$

Since eigenvalues depend continuously on α , there exists a unique $\alpha_c \in [0, 1]$ such that

$$K_{s, \text{HyIM}}^{\{\frac{\pi}{2}\}}(\alpha_c) = 0. \quad (63)$$

Finally, the optimal mixing parameter that minimizes the parameter gap is obtained by solving

$$\alpha^* = \arg \min_{\alpha \in [\alpha_c, 1]} \Delta_{\text{HyIM}}(\alpha). \quad (64)$$

SUPPLEMENTARY NOTE 6

Relationship Between the Parameter Gap and Synchronization at Bifurcation

In this section, we establish a quantitative relationship between the parameter gap and the degree of synchronization at the point of bifurcation. For the coherent Ising machine (CIM), Wang *et al.* [9] showed that when the degree of bifurcation exceeds a threshold, the binarized dominant eigenvector coincides with the optimal Ising solution. Here, we derive an analogous result for the HyIM dynamics. Specifically, we show that sufficiently strong synchronization at bifurcation ensures that the binarized dominant eigenvector attains an energy strictly below that of the first excited Ising state. We further show that the synchronization threshold increases monotonically with the HyIM parameter gap, motivating hybrid dynamics to reduce the parameter gap.

Setup and Alignment Metric

Consider the Ising Hamiltonian

$$H(\boldsymbol{\sigma}) = -\frac{1}{2}\boldsymbol{\sigma}^\top G\boldsymbol{\sigma}, \quad \boldsymbol{\sigma} \in \{-1, 1\}^N. \quad (65)$$

Let H_0 and H_1 denote the ground-state and first excited-state energies, and define the Ising energy gap $\Delta H = H_1 - H_0$.

Following [9], we quantify synchronization at bifurcation using

$$S(\mathbf{v}_{\max}) = \frac{1}{N}(\mathbf{v}_{\max}^\top \boldsymbol{\sigma}_{\max})^2, \quad \boldsymbol{\sigma}_{\max} = \text{sign}(\mathbf{v}_{\max}), \quad (66)$$

where \mathbf{v}_{\max} is the dominant eigenvector of the Jacobian evaluated at the trivial solution.

Theorem 1 *Let the first nontrivial stable state at bifurcation be proportional to the dominant eigenvector \mathbf{v}_{\max} of the Jacobian associated with the HyIM dynamics. Define the HyIM parameter gap as*

$$\Delta_{\text{HyIM}}(\alpha) = \frac{K}{2} \left[\lambda_{\max}(J_{\text{HyIM}}^{\{0, \pi\}}(\phi^*, \alpha)) + \lambda_{\max}((1 - 2\alpha)D - W) \right]. \quad (67)$$

Without loss of generality, by setting $K = 1$ and $J_{\text{HyIM}}^{\{0, \pi\}}(\phi^, \alpha) = J(\phi^*, \alpha)$, we define the parameter gap as*

$$\Delta_{\text{HyIM}}(\alpha) = \frac{1}{2} \left[\lambda_{\max}(J(\phi^*, \alpha)) + \lambda_{\max}((1 - 2\alpha)D - W) \right]. \quad (68)$$

If

$$S(\mathbf{v}_{\max}) > S_{\text{crit}}(\mathbf{v}_{\max}) = 1 - \frac{\Delta H}{N \Delta_{\text{HyIM}}(\alpha)}, \quad (69)$$

then there exists an interval $\alpha \in [0, \alpha_m]$ such that the binarized configuration $\boldsymbol{\sigma}_{\max} = \text{sign}(\mathbf{v}_{\max})$ satisfies

$$H(\boldsymbol{\sigma}_{\max}) < H_1.$$

Proof. We show that the upper bound to $H(\boldsymbol{\sigma}_{\max})$ is lesser than a lower bound to H_1 . To do this, we add and subtract the matrix $(1 - 2\alpha)D$ from Eq. 65 and rewriting $J_{\text{HyIM}}(\frac{\pi}{2}, \alpha) = (1 - 2\alpha)D - W$, we obtain,

$$H(\boldsymbol{\sigma}) = -\frac{1}{2}\boldsymbol{\sigma}^\top J_{\text{HyIM}}(\frac{\pi}{2}, \alpha)\boldsymbol{\sigma} + (1 - 2\alpha)\#\mathcal{E}(\mathcal{G}), \quad (70)$$

and define

$$H'(\boldsymbol{\sigma}) = H(\boldsymbol{\sigma}) - (1 - 2\alpha)\#\mathcal{E}(\mathcal{G}), \quad (71)$$

H' can be considered as an H with an offset.

As the matrix $J_{\text{HyIM}}(\frac{\pi}{2}, \alpha)$ is symmetric, its eigenvalue-eigenvector pair $\{(\tilde{\lambda}_i(\alpha), \mathbf{v}_i)\}_{i=1}^N$ with the following ordering $\tilde{\lambda}_{\min}(\alpha) = \tilde{\lambda}_1(\alpha) \leq \tilde{\lambda}_2(\alpha) \leq \dots \leq \tilde{\lambda}_N(\alpha) = \tilde{\lambda}_{\max}(\alpha)$. Thus, $J_{\text{OIM-DIM}}(\frac{\pi}{2}, \alpha)$ admits the spectral decomposition $J_{\text{OIM-DIM}}(\frac{\pi}{2}, \alpha) = \sum_{i=1}^N \tilde{\lambda}_i(\alpha) \mathbf{v}_i \mathbf{v}_i^\top$. Substituting this decomposition, we obtain,

$$\begin{aligned} H'(\boldsymbol{\sigma}) &= -\frac{1}{2} \sum_{i=1}^N \tilde{\lambda}_i(\alpha) (\boldsymbol{\sigma}^\top \cdot \mathbf{v}_i)^2 \\ &= -\frac{1}{2} \left(\tilde{\lambda}_{\max}(\alpha) (\boldsymbol{\sigma}^\top \cdot \mathbf{v}_{\max})^2 + \sum_{i=1}^{N-1} \tilde{\lambda}_i(\alpha) (\boldsymbol{\sigma}^\top \cdot \mathbf{v}_i)^2 \right) \\ &= -\frac{1}{2} \left(\tilde{\lambda}_{\max}(\alpha) \left(N - \sum_{i=1}^{N-1} (\boldsymbol{\sigma}^\top \mathbf{v}_i)^2 \right) + \sum_{i=1}^{N-1} \tilde{\lambda}_i(\alpha) (\boldsymbol{\sigma}^\top \mathbf{v}_i)^2 \right) \\ &= -\frac{1}{2} N \tilde{\lambda}_{\max}(\alpha) + \frac{1}{2} \sum_{i=1}^{N-1} \Delta_i (\boldsymbol{\sigma}^\top \mathbf{v}_i)^2, \end{aligned} \quad (72)$$

where $\Delta_i = \tilde{\lambda}_{\max}(\alpha) - \tilde{\lambda}_i(\alpha)$ and $\Delta_i \geq \Delta_{i+1} \geq 0$, and from Eq.71, we can get

$$H_0 \geq -\frac{N}{2} \tilde{\lambda}_{\max}(\alpha) + (1 - 2\alpha) \# \mathcal{E}(\mathcal{G}). \quad (74)$$

To derive an upper bound on $H'(\boldsymbol{\sigma})$, we further analyze Eq. 72 by adding and subtracting the term $\frac{N}{2} \lambda_{\max}(J_{\text{HyIM}}(\phi^*, \alpha))$. For notational simplicity, we denote $J_{\text{HyIM}}(\phi^*, \alpha) \equiv J_{\text{HyIM}}^\Phi$.

$$\begin{aligned} H'(\boldsymbol{\sigma}) &= -\frac{1}{2} \boldsymbol{\sigma}^\top \left(\lambda_{\max}(J_{\text{HyIM}}^\Phi) I + \sum_{i=1}^N \tilde{\lambda}_i(\alpha) \mathbf{v}_i \mathbf{v}_i^\top \right) \boldsymbol{\sigma} + \lambda_{\max}(J_{\text{HyIM}}^\Phi) \frac{N}{2} \\ &= -\frac{1}{2} \lambda_{\max}(J_{\text{HyIM}}^\Phi) \left(\sum_{i=1}^N (\mathbf{v}_i^\top \boldsymbol{\sigma})^2 \right) - \frac{1}{2} \sum_{i=1}^N \tilde{\lambda}_i(\alpha) (\mathbf{v}_i^\top \boldsymbol{\sigma})^2 + \lambda_{\max}(J_{\text{HyIM}}^\Phi) \frac{N}{2} \\ &= -\frac{1}{2} \sum_{i=1}^N \left(\tilde{\lambda}_i(\alpha) + \lambda_{\max}(J_{\text{HyIM}}^\Phi) \right) (\mathbf{v}_i^\top \boldsymbol{\sigma})^2 + \lambda_{\max}(J_{\text{HyIM}}^\Phi) \frac{N}{2} \end{aligned} \quad (75)$$

$$\leq -\frac{1}{2} \left(\tilde{\lambda}_{\max}(\alpha) + \lambda_{\max}(J_{\text{HyIM}}^\Phi) \right) (\mathbf{v}_{\max}^\top \boldsymbol{\sigma})^2 + \lambda_{\max}(J_{\text{HyIM}}^\Phi) \frac{N}{2} \quad (76)$$

The inequality in Eq. (76) follows from Eq. (75) by restricting α to values that satisfy the following inequality.

$$\begin{aligned} \sum_{i=1}^N \left(\tilde{\lambda}_i(\alpha) + \lambda_{\max}(J_{\text{HyIM}}^\Phi) \right) (\mathbf{v}_i^\top \boldsymbol{\sigma})^2 &\geq \left(\tilde{\lambda}_{\max}(\alpha) + \lambda_{\max}(J_{\text{HyIM}}^\Phi) \right) (\mathbf{v}_{\max}^\top \boldsymbol{\sigma})^2, \\ \sum_{i=1}^{N-1} \left(\tilde{\lambda}_i(\alpha) + \lambda_{\max}(J_{\text{HyIM}}^\Phi) \right) (\mathbf{v}_i^\top \boldsymbol{\sigma})^2 &\geq 0 \end{aligned} \quad (77)$$

We now establish the existence of a critical value $\alpha \in [0, \alpha_m]$ such that Eq. (77) holds.

Since $(\mathbf{v}_i^\top \boldsymbol{\sigma})^2 \geq 0$ for all i and $\lambda_{\max}(J_{\text{HyIM}}^\Phi) \geq 0$, a sufficient condition for the inequality to hold is

$$\tilde{\lambda}_{\min}(\alpha) + \lambda_{\max}(J_{\text{HyIM}}^\Phi) \geq 0 \iff \tilde{\lambda}_{\min}(\alpha) \geq -\lambda_{\max}(J_{\text{HyIM}}^\Phi) \quad (78)$$

Similarly, we can show that $\tilde{\lambda}_{\min}(\alpha)$ is decreasing in α . Consider $0 < \alpha_1 < \alpha_2 < 1$. Then,

$$\begin{aligned} \tilde{\lambda}_{\min}((1 - 2\alpha_1)D - W) - \tilde{\lambda}_{\min}((1 - 2\alpha_2)D - W) &= \tilde{\lambda}_{\min}((1 - 2\alpha_1)D - W) + \tilde{\lambda}_{\max}(-(1 - 2\alpha_2)D + W) \\ &\geq \tilde{\lambda}_{\min}((1 - 2\alpha_1)D - W - (1 - 2\alpha_2)D + W) \\ &\geq \tilde{\lambda}_{\min}(2(\alpha_2 - \alpha_1)D) = 2(\alpha_2 - \alpha_1) \min_{1 \leq i \leq N} d_i \geq 0, \end{aligned} \quad (79)$$

This shows that $\tilde{\lambda}_{\min}(\alpha)$ is monotone decreasing in α .

We further note that when $\alpha = 0$, the HyIM model reduces to the pure OIM model. In this case, the minimum eigenvalue satisfies $\tilde{\lambda}_{\min}(0) = 0$, (since $D - W \succeq 0$). Moreover, $\tilde{\lambda}_{\min}(\alpha)$ is concave in α , meaning that there exists a range of $\alpha \in [0, \alpha_m]$ such that the sufficient condition in Eq. 78 holds, which implies that there exists a range of α for which the inequality in Eq. (76) is satisfied.

Therefore, substituting Eq. 76 to Eq. 71 we get,

$$\begin{aligned}
H(\boldsymbol{\sigma}_{max}) &= H'(\boldsymbol{\sigma}_{max}) + (1 - 2\alpha)\#\mathcal{E}(\mathcal{G}) \\
&\leq -\frac{1}{2}\left(\tilde{\lambda}_{\max} + \tilde{\lambda}_{\max}(J_{\text{HyIM}}^{\Phi})\right)(\mathbf{v}_{\max}^{\top}\boldsymbol{\sigma}_{max})^2 + \tilde{\lambda}_{\max}(J_{\text{HyIM}}^{\Phi})\frac{N}{2} + (1 - 2\alpha)\#\mathcal{E}(\mathcal{G}) \\
&< -\frac{N}{2}\left(\tilde{\lambda}_{\max} + \tilde{\lambda}_{\max}(J_{\text{HyIM}}^{\Phi})\right) + \Delta H + \tilde{\lambda}_{\max}(J_{\text{HyIM}}^{\Phi})\frac{N}{2} + (1 - 2\alpha)\#\mathcal{E}(\mathcal{G}) \\
&< H_1 - H_0 - \frac{N}{2}\tilde{\lambda}_{\max} + (1 - 2\alpha)\#\mathcal{E}(\mathcal{G}).
\end{aligned} \tag{80}$$

Eq. 80 is obtained by substituting $(\mathbf{v}_{\max}^{\top}\boldsymbol{\sigma}_{max})^2$ using the relationships given in Eq. 66 and Eq. 69.

Now we observe the following inequality using $H_0 \geq -\frac{N}{2}\tilde{\lambda}_{\max} + (1 - 2\alpha)\#\mathcal{E}(\mathcal{G})$ from (74), therefore

$$H(\boldsymbol{\sigma}_{max}) < H_1,$$

which completes the proof. ■

Interplay Between α_c and α_m

Two critical parameters arise in the analysis: α_c , defined as the value at which the trivial state loses stability at $K_s = 0$, and α_m , defined as the maximal value of α for which, given the alignment condition

$$S(\mathbf{v}_{\max}) > S_{\text{crit}}(\mathbf{v}_{\max}) = 1 - \frac{\Delta H}{N \Delta_{\text{HyIM}}(\alpha)}, \tag{81}$$

the dominant eigenmode satisfies

$$H(\boldsymbol{\sigma}_{\max}) < H_1.$$

Two distinct cases emerge for critical values of α_m and α_c .

- **Case 1:** $\alpha_m > \alpha_c$.

In this case, there exists an interval $\alpha \in [\alpha_c, \alpha_m]$ such that

$$H(\boldsymbol{\sigma}_{\max}) < H_1.$$

Thus, once the trivial state loses stability at α_c , the dynamics evolve along the dominant eigenmode toward the ground state. Ground-state recovery is therefore guaranteed.

- **Case 2:** $\alpha_m < \alpha_c$.

In this case, the dominant-eigenmode criterion does not guarantee ground-state recovery at the bifurcation point. However, the admissible range of α_m may extend beyond its initial threshold via modifying Eq. 81 as

$$S(\mathbf{v}_{\max}) > S_{\text{crit},k}(\mathbf{v}_{\max}) = 1 - \frac{\Delta H^k}{N \Delta(\mathcal{G}, \alpha)}, \tag{82}$$

where H^k denotes the k^{th} excited state and $\Delta H^k = H^k - H_0$. The extension of α_m can be characterized by the modified Eq. 80 as

$$H(\boldsymbol{\sigma}_{\max}) < H^k - H_0 - \frac{N}{2}\tilde{\lambda}_{\max} + (1 - 2\alpha)\#\mathcal{E}(\mathcal{G}). \tag{83}$$

As α increases, both $\tilde{\lambda}_{\max}$ and the term $(1 - 2\alpha)\#\mathcal{E}(\mathcal{G})$ decrease monotonically. Consequently, the inequality can be satisfied successively for higher excited states for k such that $\alpha_m^k > \alpha_c$, if \mathbf{v}_{\max} satisfies Eq. (82), then it must correspond to a spin configuration $\boldsymbol{\sigma}_{\max}$ satisfying

$$H(\boldsymbol{\sigma}_{\max}) < H^k. \quad (84)$$

We now examine the relationship between α_c and α_m for bipartite graphs.

Lemma 3 (Critical parameters (α_c, α_m) for bipartite graphs) *Let $\mathcal{G} = (\mathcal{V}, \mathcal{E})$ be a connected bipartite graph with degree matrix D and weight matrix W . Consider the HyIM model evaluated at $\phi = \frac{\pi}{2}$.*

Then the following hold:

(i) *The critical parameter α_c , defined as the K_s at which the trivial state loses stability,*

$$\lambda_{\max}((1 - 2\alpha)D - W) = 0,$$

satisfies

$$\alpha_c = 1.$$

(ii) *The maximal admissible parameter α_m , determined by the condition*

$$\sum_{i=1}^{N-1} \left(\tilde{\lambda}_i(\alpha) + \lambda_{\max}(J_{\text{HyIM}}^{\Phi}) \right) (\mathbf{v}_i^{\top} \boldsymbol{\sigma})^2 \geq 0,$$

satisfies

$$\alpha_m = 1.$$

Consequently,

$$\alpha_c = \alpha_m = 1.$$

Proof.

(a) Derivation of α_c for a bipartite graph.

The critical value α_c is determined by the condition $K_s = 0$, which corresponds to the point where the trivial state loses stability and the dominant eigenmode emerges.

From the definition,

$$K_{s, \text{HyIM}}^{\{\frac{\pi}{2}\}}(\alpha) = -\frac{K}{2} \lambda_{\max}((1 - 2\alpha)D - W). \quad (85)$$

Hence, α_c satisfies

$$\lambda_{\max}((1 - 2\alpha)D - W) = 0.$$

For a bipartite graph, the eigenvector associated with the largest eigenvalue is aligned with the ground-state configuration (see Lemma 1 in Supplementary Note 3). Due to the block structure of a bipartite graph, this eigenvector can be written as

$$\mathbf{v}_{\max} \propto \boldsymbol{\sigma}^* = \begin{pmatrix} \mathbf{1}_m \\ -\mathbf{1}_n \end{pmatrix}.$$

We evaluate the action of $(1 - 2\alpha)D - W$ on this vector:

$$\begin{aligned} ((1 - 2\alpha)D - W) \begin{pmatrix} \mathbf{1}_m \\ -\mathbf{1}_n \end{pmatrix} &= \begin{pmatrix} (1 - 2\alpha)D_1 & -W \\ -W^{\top} & (1 - 2\alpha)D_2 \end{pmatrix} \begin{pmatrix} \mathbf{1}_m \\ -\mathbf{1}_n \end{pmatrix} \\ &= (1 - 2\alpha) \begin{pmatrix} D_1 \mathbf{1}_m \\ -D_2 \mathbf{1}_n \end{pmatrix} + \begin{pmatrix} W \mathbf{1}_n \\ -W^{\top} \mathbf{1}_m \end{pmatrix}. \end{aligned} \quad (86)$$

Here, D_1 and D_2 denote the diagonal degree matrices corresponding to the two partitions of the bipartite graph. Since the graph is bipartite, the degree relations satisfy

$$D_1 \mathbf{1}_m = W \mathbf{1}_n, \quad D_2 \mathbf{1}_n = W^\top \mathbf{1}_m.$$

Substituting these identities yields

$$\begin{aligned} ((1-2\alpha)D - W)\boldsymbol{\sigma}^* &= (1-2\alpha) \begin{pmatrix} D_1 \mathbf{1}_m \\ -D_2 \mathbf{1}_n \end{pmatrix} + \begin{pmatrix} D_1 \mathbf{1}_m \\ -D_2 \mathbf{1}_n \end{pmatrix} \\ &= 2(1-\alpha) \begin{pmatrix} D_1 \mathbf{1}_m \\ -D_2 \mathbf{1}_n \end{pmatrix} \\ &= 2(1-\alpha)D \boldsymbol{\sigma}^*. \end{aligned} \tag{87}$$

Thus, $\boldsymbol{\sigma}^*$ is an eigenvector with eigenvalue

$$\lambda_{\max} = 2(1-\alpha)d,$$

where d denotes the degree (or, more generally, the action of D on the vector).

The largest eigenvalue vanishes when

$$2(1-\alpha_c) = 0,$$

which implies

$$\alpha_c = 1.$$

(b) Derivation of α_m for a bipartite graph.

The critical value α_m is determined by the sufficient condition given in Eq. (77), namely

$$\sum_{i=1}^{N-1} \left(\tilde{\lambda}_i(\alpha) + \lambda_{\max}(J_{\text{HyIM}}^\Phi) \right) (\mathbf{v}_i^\top \boldsymbol{\sigma})^2 \geq 0. \tag{88}$$

From Lemma 1 (Supplementary Note 3), for bipartite graphs the case $\alpha = 1$ (i.e., HyIM reduces to pure DIM) we obtain

$$(\mathbf{v}_i^\top \boldsymbol{\sigma})^2 = 0, \quad i = 1, 2, \dots, N-1.$$

We now verify whether the synchronization condition

$$S(\mathbf{v}_{\max}) = \frac{1}{N} (\mathbf{v}_{\max}^\top \boldsymbol{\sigma}_{\max})^2 > 1 - \frac{\Delta H}{N \Delta_{\text{HyIM}}(\alpha)} \tag{89}$$

holds for bipartite graphs at $\alpha = 1$. This is equivalent to showing that

$$\frac{1}{N} (\mathbf{v}_{\max}^\top \boldsymbol{\sigma}_{\max})^2 - 1 + \frac{\Delta H}{N \Delta_{\text{HyIM}}(\alpha)} > 0. \tag{90}$$

For bipartite graphs, the dominant eigenvector \mathbf{v}_{\max} coincides with $\boldsymbol{\sigma}_{\max}$ at $\alpha = 1$, implying

$$\frac{1}{N} (\mathbf{v}_{\max}^\top \boldsymbol{\sigma}_{\max})^2 = 1.$$

Hence, the condition reduces to

$$\frac{\Delta H}{N \Delta_{\text{HyIM}}(\alpha)} > 0. \tag{91}$$

Since both ΔH and $\Delta_{\text{HyIM}}(\alpha)$ are non-negative, the inequality satisfies. Therefore, the synchronization condition holds for $\alpha = 1$, implying

$$\alpha_m = 1.$$

From parts (a) and (b), since $\alpha_c = 1$ and $\alpha_m = 1$, we conclude that

$$\alpha_c = \alpha_m = 1,$$

which completes the proof. ■

We now illustrate the synchronization measures $S(\mathbf{v}_{max})$ and $S_{crit}(\mathbf{v}_{max})$ for Möbius ladder graphs for the first excited state as a function of $\alpha \in [0, 1]$, for system sizes $6 \leq N \leq 16$.

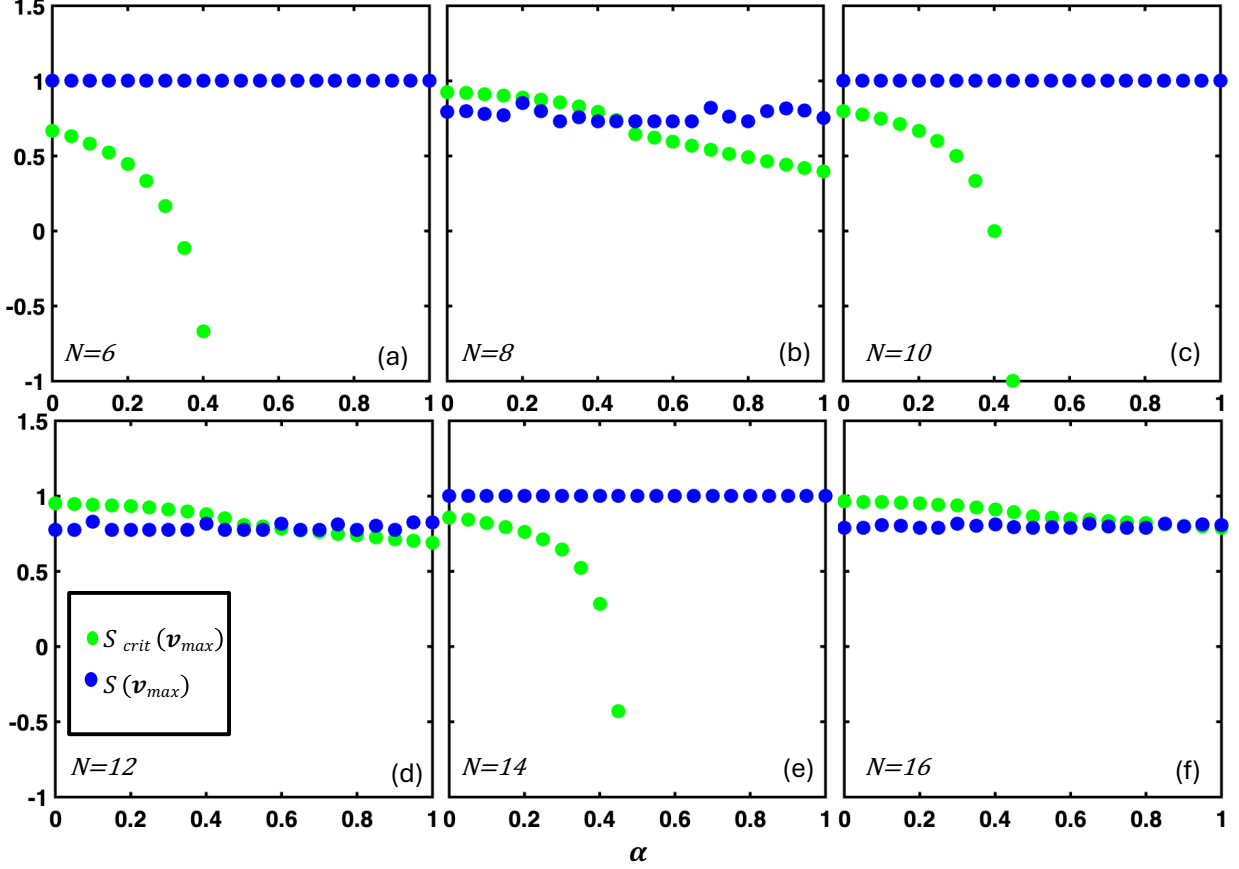


FIG. 3: Evolution of $S(\mathbf{v}_{max})$ and $S_{crit}(\mathbf{v}_{max})$ with α for Möbius ladder graphs of different sizes (a) $N = 6$, (b) $N = 8$, (c) $N = 10$, (d) $N = 12$, (e) $N = 14$, and (f) $N = 16$.

SUPPLEMENTARY NOTE 7

Simulation Parameters and Experimental Settings

This section summarizes the numerical parameters and experimental settings used in all simulations presented in the main text. For each model, we specify the system parameters, initialization conditions, and time-dependent control parameters employed in the simulations. Unless otherwise stated, the parameters listed here are held fixed across all realizations to ensure consistency and reproducibility of the reported results.

Table II summarizes the simulation parameters and control protocols used to generate the results shown in Fig. 1 of the main text. For each model (DIM, OIM, CIM, and SBM).

TABLE II: Simulation parameters used in Figure 1 of the main text.

Model	Parameters	Control Parameter ($\eta(t)$)
	$K = 1$	
DIM	$t_{\text{stop}} = 40$ $A_n = 10^{-3}$	$K_s(t) = \frac{4t}{t_{\text{stop}}}$
	$K = 1$	
OIM	$t_{\text{stop}} = 40$ $A_n = 10^{-3}$	$K_s(t) = \frac{4t}{t_{\text{stop}}}$
	$\xi = 0.05$	
CIM	$t_{\text{stop}} = 40$ $A_n = 10^{-3}$	$p(t) = \frac{4t}{t_{\text{stop}}}$
	$K_e = 1.0$	
	$\xi_0 = 0.05$	
SBM	$\Delta = 1$ $t_{\text{stop}} = 40$ $A_n = 10^{-3}$	$p(t) = \frac{4t}{t_{\text{stop}}}$

Table III summarizes the simulation parameters and control protocols used to generate the results shown in Fig. 2(b) of the main text.

TABLE III: Simulation parameters used in Figure 2(b) of the main text.

Model	Parameters	Control Parameter ($\eta(t)$)
	$K = 1$	
HyIM	$t_{\text{stop}} = 4$ $A_n = 10^{-4}$	$K_s(t) = K_s(t_0) + \frac{15t}{t_{\text{stop}}}$
	$K_s(t_0) = \max\{0, \lambda_{\max}(J_{\text{HyIM}}(\frac{\pi}{2}, \alpha)) - 3\}$.	

Figure 4 shows the distribution of the δ as a function of the parameter α for individual graphs G1–G5 [17], complementing the collective distribution shown in Fig. 2(b) of the main text. For each graph, box plots summarize the results from 10 independent simulation trials at each value of α .

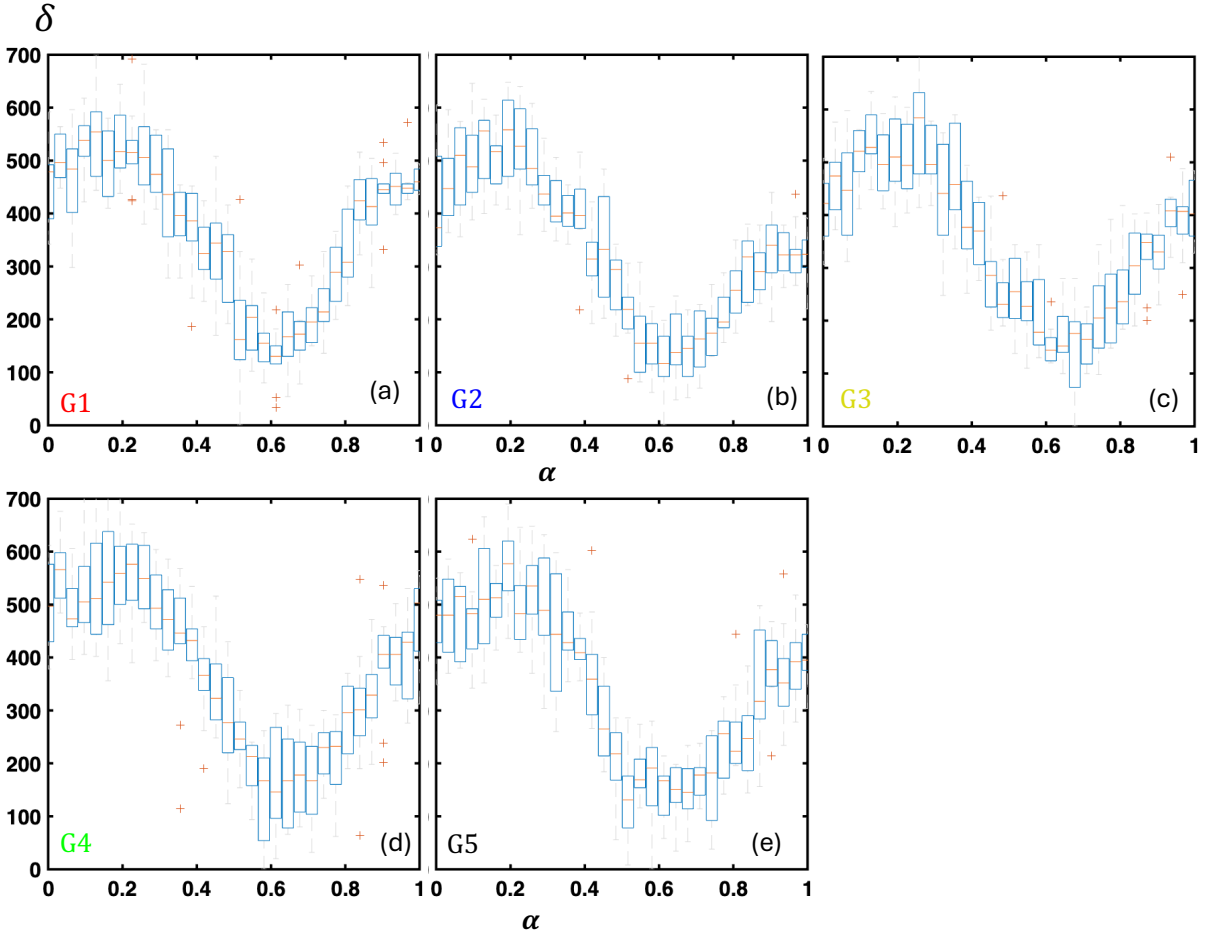


FIG. 4: Box-plot showing distribution of δ for (a) G1, (b) G2, (c) G3, (d) G4, (e) G5 graphs. Each graph is simulated for 10 independent trials.